Supplementary Information for

Statistical inference of keystone taxa reshaping the assembly rules of forest root microbiomes

Mikihito Noguchi[1-3], Kenta Suzuki[4,5], Hiroaki Fujita[2,6], and Hirokazu Toju[2,6]

[1]Center for Ecological Research, Kyoto University, Otsu, Shiga 520-2133, Japan

[2]Laboratory of Ecosystems and Coevolution, Graduate School of Biostudies, Kyoto University, Kyoto 606-8501, Japan

[3]Research Fellow of Japan Society for the Promotion of Science, Tokyo, Japan

[4]Integrated Bioresource Information Division, BioResource Research Center, RIKEN, Tsukuba, Ibaraki 305-0074, Japan.

[5]Institute for Multidisciplinary Sciences, Yokohama National University, Yokohama, Kanagawa 240-8501, Japan.

[6]Center for Living Systems Information Science (CeLiSIS), Graduate School of Biostudies, Kyoto University, Kyoto 606-8501, Japan

Correspondence:

Mikihito Noguchi: noguchi.mikihito.57s@st.kyoto-u.ac.jp

Hirokazu Toju: toju.hirokazu.4c@kyoto-u.ac.jp

Supplementary Methods

Root microbiome data

We compiled the root-tip fungal community datasets described in our previous study with newly obtained prokaryotic data[1]. Briefly, root-tip samples (1 cm terminal roots) were sampled in the research forest of Sugadaira Research Station, Mountain Science Center, University of Tsukuba, Ueda, Nagano Prefecture, Japan (36.524 ºN; 138.349 ºE; 1,340 m a.s.l.). The root tips were sonicated in 0.5% tween 20 and surface sterilized subsequently with NaClO (Nakalaitesque, effective chlorine concentration ca. 11%) diluted to 1% (v/v), sterile distilled water (three times), and 99.5% ethanol[1]. After DNA extraction with a cetyltrimethylammonium bromide (CTAB) method, the internal transcribed spacer (ITS) region of fungi and the 16S rRNA region of prokaryotes were PCR-amplified and the purified amplicons were sequenced in an Illumina MiSeq sequener[1]. The obtained 134,066,687 and 73,183,237 sequencing reads of ITS and 16S rRNA region were converted into FASTQ files using bcl2fastq (version 1.8.4) and demultiplexed with Claident v0.9.2022.01.26[2,3]. From these outputs, amplicon sequence variants (ASVs) were constructed by adaptor trimming by Cutadapt[4] (version. 3.7), quality filtering and denoising by DADA2[5] v.1.18.0 of R 4.2.2[6]. Contaminant ASVs were removed with the R package "decontam" (the method "prevalence") [7]. Taking into account duplication error in PCR, the ASVs were re-clustered into operational taxonomic units (OTUs) with a 97% similarity threshold using the program VSEARCH v2.21.1[8]. The taxonomic assignments of fungal and prokaryotic OTUs were performed based on the UNITE[9] general FASTA release for eukaryotes 2. Version 18.07.2023 and the SILVA[10] version 138 database using the naive Bayesian classifier method in DADA2[5,11]. The root sample which had less than 1,000 fungal/prokaryotic reads were discarded. Then, obtained fungal/prokaryotic OTU matrices of the samples whose host plants (described elsewhere[1]) were detected more than 50 times (*Acer*, *Betula*, *Juglans*, *Larix*, *Pinus* and *Populus*) were rarefied with coverage-based method using "vegan" package v.2.6-8[12]. In total, both fungal and prokaryotic community data were obtained for 1,270 root samples collected from the 125 sampling points. In total, 2,249 fungal and 12,479 prokaryotic OTUs were obtained from those root samples.

Host preference of the fungal/prokaryotic families

To evaluate the host specificity of the fungal and prokaryotic families used in energy landscape estimation, we calculated the *d′* metrics of interaction specificity[13] and two dimensional preference of plant fungal associations (*2DP*)[14] for the 34 fungal and 45 prokaryotic families (selected in Supplementary Figs. S1, S3) with the same way as our previous study[1]. In this analyses, the fungal/prokaryotic community data were binarized with the same criteria as energy landscape analysis (described detail below). The standardized indices and their statistical significances were assessed by comparing the observed data with null model simulations. Specifically, the host plant information was shuffled among root samples collected at the same sampling positions (10,000 permutations), and the

indices calculated from the randomized datasets were compared to the original one. For each fungal and prokaryotic family, a standardized d' metrics was calculated as follows:

$$[d'_{\text{original}} - \text{Mean}\,(d'_{\text{randomized}})] \,/\, \text{SD}\,(d'_{\text{randomized}}),$$

where d'_{original} was the d' estimate of the original data and Mean ($d'_{\text{randomized}}$) and SD ($d'_{\text{randomized}}$) were the mean and standard deviation of the d' of randomized data matrices. For each pair of six host plants and fungal/prokaryotic family, standardized *2DP* was also calculated as follows:

$$[N_{\text{original}}\,(i,j) - \text{Mean}\,(N_{\text{randomized}}\,(i,j))] \,/\, \text{SD}\,(N_{\text{randomized}}\,(i,j)),$$

where $N_{\text{original}}\,(i,j)$ denoted the number of root samples from which a focal combination of a symbiont family and a host plant was observed in the original data, and the Mean ($N_{\text{randomized}}\,(i,j)$) and SD ($N_{\text{randomized}}\,(i,j)$) were the mean and standard deviation of the number of samples for the focal symbiont-plant pair across randomized matrices. False discovery rates [FDR[15]] were also calculated to evaluate the statistical significance of the two indices (d' metrics ; one-tailed tests, *2DP*; two-tailed tests).

Preparation of data matrices for energy landscape analysis

After excluding five and three samples in which more than 50% of sequence reads could not be annotated at the family level in fungal and prokaryotic communities respectively, the fungal and prokaryotic data matrices were converted into a binary format. The threshold of the binarization was set as $Mean(\log(X_i)) - 2\,SD(\log(X_i))$, where X_i denotes the read counts of taxon i across the samples in which it was detected. To make exploration within assembly graphs (2^S possible community states, where S is the number of taxa) computationally feasible, we prioritized and selected families, respectively, in the fungal and prokaryotic data. Specifically, a series of permutational analyses of variance (PerMANOVA)[16] was performed for the relative abundance matrix of fungal or prokaryotic data by setting the presence/absence of a target family as an explanatory variable (10,000 iterations). In the PerMANOVA, the Bray-Curtis metric was used to calculate community dissimilarity between root samples, and the host plants and sampling points were set as additional explanatory variables (i.e., covariates). Families were then ordered depending on their explanatory power (R^2) in the PerMANOVA. The optimal set (number) of families to be analyzed in the energy landscape analysis was subsequently explored for the fungal and prokaryotic data, respectively. To apply a simple criterion, we evaluated correspondence between the community dissimilarity values calculated based on the original relative abundance data (Bray-Curtis distance for quantitative data) and those calculated based on the binarized data (Jaccard distance for binary data). An optimal binarized data matrix (sets of families) preserving the information of original relative abundance data was selected based on the Kendall's rank correlation coefficient for the correspondence between quantitative and binary data.

Supplementary references

1. Noguchi, M. & Toju, H. Mycorrhizal and endophytic fungi structure forest below-ground symbiosis through contrasting but interdependent assembly processes. *Environ. Microbiome* **19**, 84 (2024).

2. Tanabe, A. S. & Toju, H. Two New Computational Methods for Universal DNA Barcoding: A Benchmark Using Barcode Sequences of Bacteria, Archaea, Animals, Fungi, and Land Plants. *PLoS ONE* **8**, e76910 (2013).

3. Tanabe, A. S. Claident v0.9.2022.01.26. 2022. (2022).

4. Martin, M. Cutadapt removes adapter sequences from high-throughput sequencing reads. *EMBnet.journal* **17**, 10–12 (2011).

5. Callahan, B. J. *et al.* DADA2: High-resolution sample inference from Illumina amplicon data. *Nat. Methods* **13**, 581–583 (2016).

6. R Core Team. R: A language and environment for statistical computing. (2022).

7. Davis, N. M., Proctor, D. M., Holmes, S. P., Relman, D. A. & Callahan, B. J. Simple statistical identification and removal of contaminant sequences in marker-gene and metagenomics data. *Microbiome* **6**, 226 (2018).

8. Rognes, T., Flouri, T., Nichols, B., Quince, C. & Mahé, F. VSEARCH: a versatile open source tool for metagenomics. *PeerJ* **4**, e2584 (2016).

9. Abarenkov, K. *et al.* UNITE general FASTA release for eukaryotes 2. UNITE Community. https://doi.org/10.15156/BIO/2938070 (2023).

10. Quast, C. *et al.* The SILVA ribosomal RNA gene database project: improved data processing and web-based tools. *Nucleic Acids Res.* **41**, D590–D596 (2013).

11. Wang, Q., Garrity, G. M., Tiedje, J. M. & Cole, J. R. Naïve Bayesian Classifier for Rapid Assignment of rRNA Sequences into the New Bacterial Taxonomy. *Appl. Environ. Microbiol.* **73**, 5261–5267 (2007).

12. Oksanen, O. *et al.* vegan: Community Ecology Package. (2022).

13. Blüthgen, N., Menzel, F., Hovestadt, T., Fiala, B. & Blüthgen, N. Specialization, Constraints, and

Conflicting Interests in Mutualistic Networks. *Curr. Biol.* **17**, 341–346 (2007).

14. Toju, H., Tanabe, A. S. & Ishii, H. S. Ericaceous plant–fungus network in a harsh alpine–subalpine environment. *Mol. Ecol.* **25**, 3242–3257 (2016).

15. Benjamini, Y. & Hochberg, Y. Controlling the False Discovery Rate: A Practical and Powerful Approach to Multiple Testing. *J. R. Stat. Soc. Ser. B Methodol.* **57**, 289–300 (1995).

16. Anderson, M. J. A new method for non-parametric multivariate analysis of variance. *Austral Ecol.* **26**, 32–46 (2001).

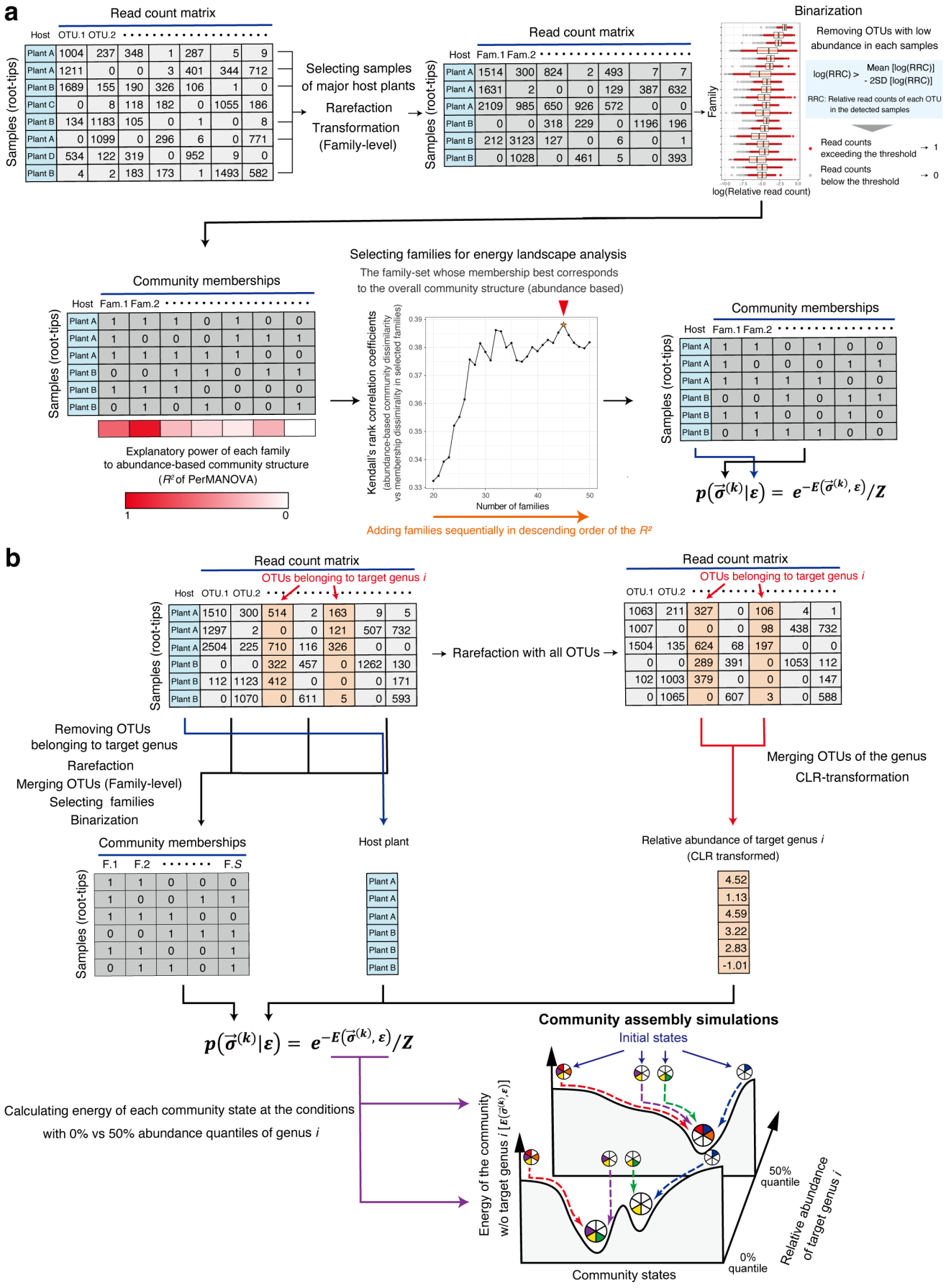

Supplementary Fig. S1 | Workflow for energy landscape analysis and evaluation of "keystoneness" (**a**) Input data for energy landscape analysis. We performed coverage-based

rarefaction for the root samples. In a matrix of family-level taxonomic compositions, relative read counts of each family were binarized with a threshold described in Methods and Supplementary Figure S2. To make the subsequent statistical analysis (energy landscape analysis) computationally feasible, we prioritized and selected families based on their contribution to overall community structure, evaluated by PerMANOVA (R^2; Supplementary Tables S1 and S2). The family set showing the highest correspondence between its binarized pattern and the abundance-based community structure was selected among candidate sets determined by their R^2 values. Energy landscape analysis was then conducted using the family-set with host plant genera (encoded as dummy variables) as explanatory variables. (**b**) Input data for the keystone exploration. From the original data matrix excluding OTUs annotated as a focal genus, coverage-based rarefaction was conducted. Binarization was applied to the same set of families as in (**a**). In parallel, the whole community matrix was rarefied, and the genus-level compositions were subjected to CLR transformation. Energy landscape analysis was performed by including host plant genera (dummy variables) and CLR-transformed relative read counts (+1) of the focal genus as external factors. Two types of indices for identifying potential keystone taxa were calculated by comparing the landscape topography inferred in the absence of the focal species/taxon with that estimated under the assumption of an intermediate abundance level (25%, 50%, or 75% quantiles of abundance across samples in which the focal taxon was present) (Fig. 1g).

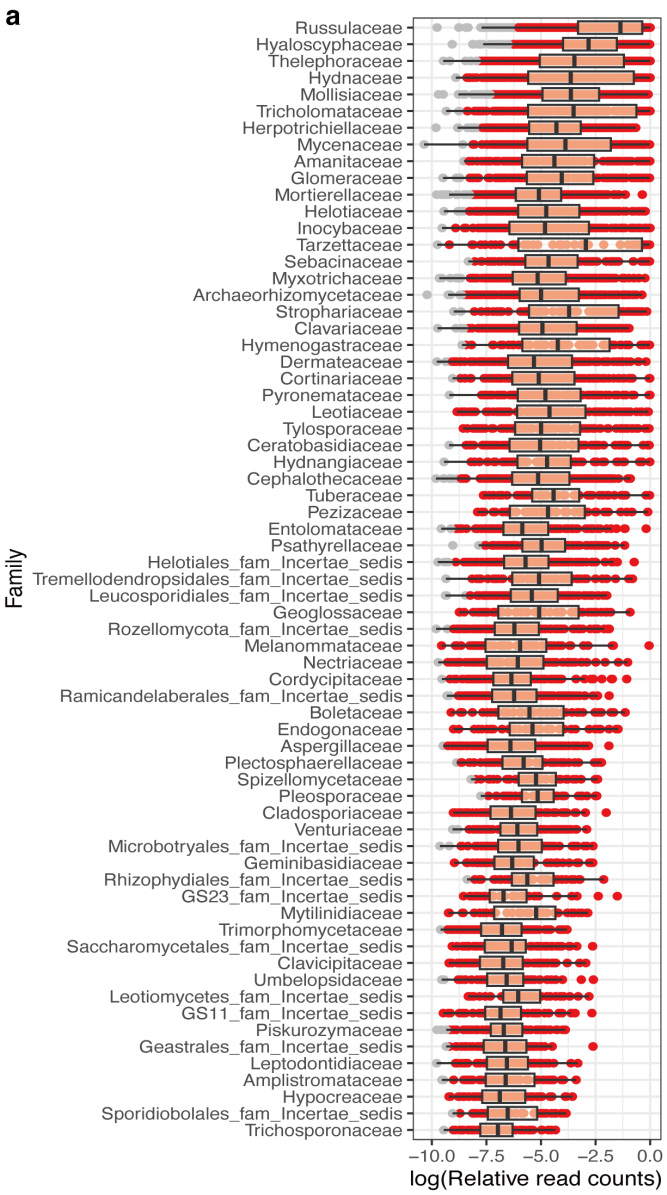

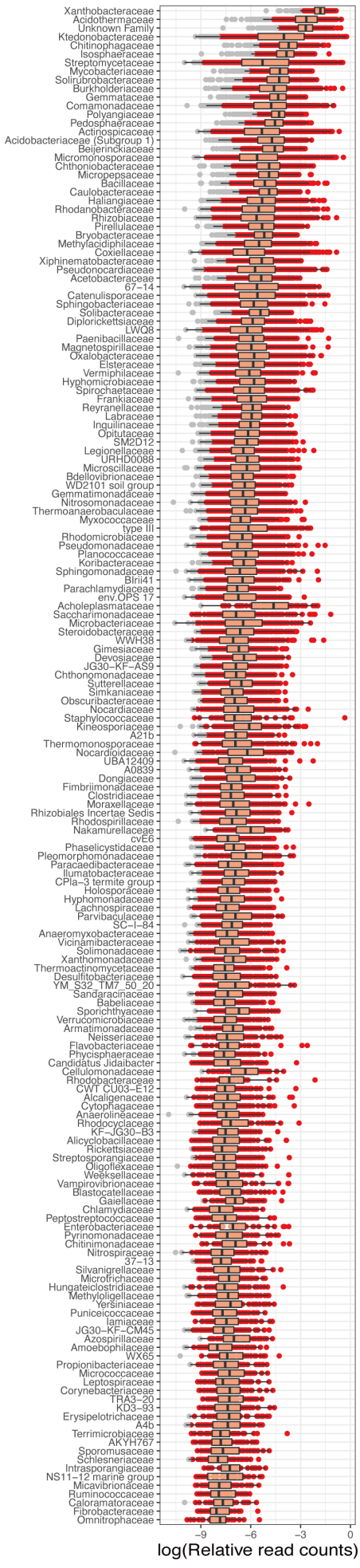

Binarization thresholds for energy landscape analysis

log(RRC) > Mean [log(RRC)] - 2SD [log(RRC)]

RRC: Relative read counts of each OTU in the detected samples

Read counts exceeding the threshold

Read counts below the threshold

Supplementary Fig. S2 | Relative abundances of microbial families | (**a**) Distribution of relative read counts of each fungal family in samples from which it was detected. To remove potential sequencing contaminants, the threshold for binarization was defined for each family as Mean [log (RRC)] – 2SD [log (RRC)], where Mean [log (RRC)] and SD [log (RRC)] denote the mean and standard deviation of the log-transformed relative read counts of the focal family, respectively. (**b**) Distribution of relative read counts for each prokaryotic family.

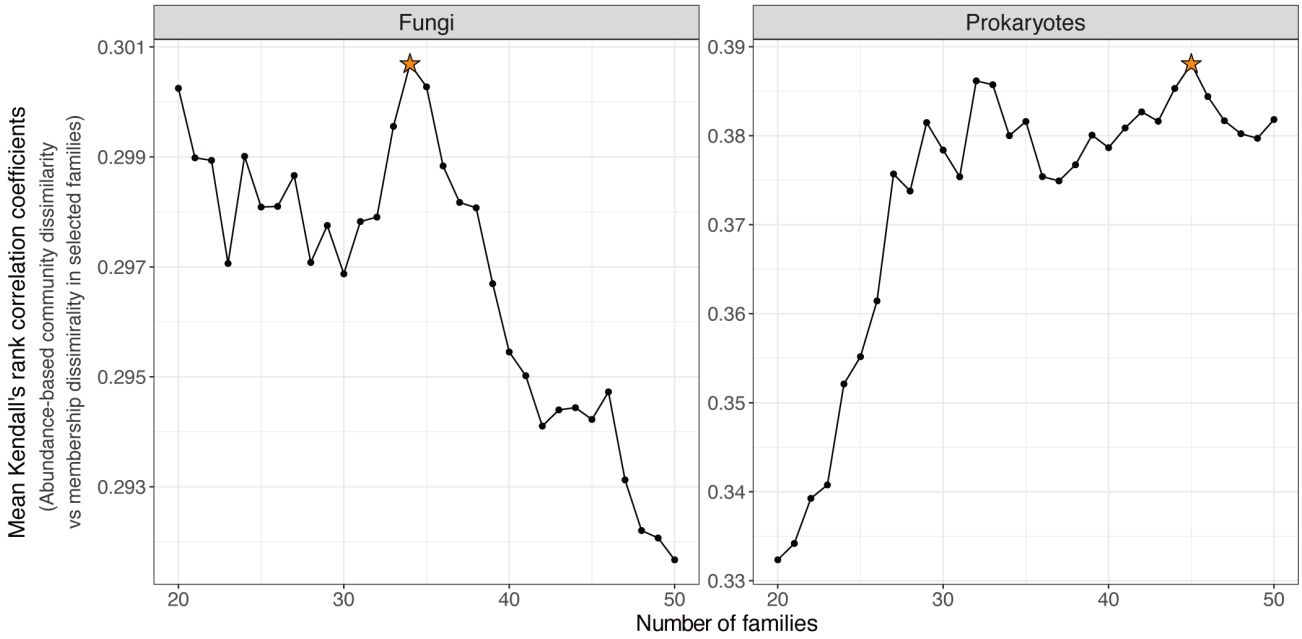

158

159 **Supplementary Fig. S3 | Selecting optimal family sets for energy landscape analysis.** The optimal
160 sets (numbers) of fungal and prokaryotic families were determined to best preserve the information
161 contained in the original community data during the filtering process for energy landscape analysis
162 (see Supplementary Fig. S1 and Methods for details). Specifically, to make the exploration of optimal
163 fungal and prokaryotic family sets computationally feasible, we first ordered 50 families based on
164 their explanatory power for the overall community structure (R^2 in the PerMANOVA; see
165 Supplementary Tables S1 and S2). We then evaluated the correlations between community
166 dissimilarity values calculated from the binarized data of each candidate family set (Jaccard distance)
167 and those calculated from the original relative abundance data (Bray–Curtis distance). The selected
168 fungal and prokaryotic family sets are indicated by star-shaped symbols.

169

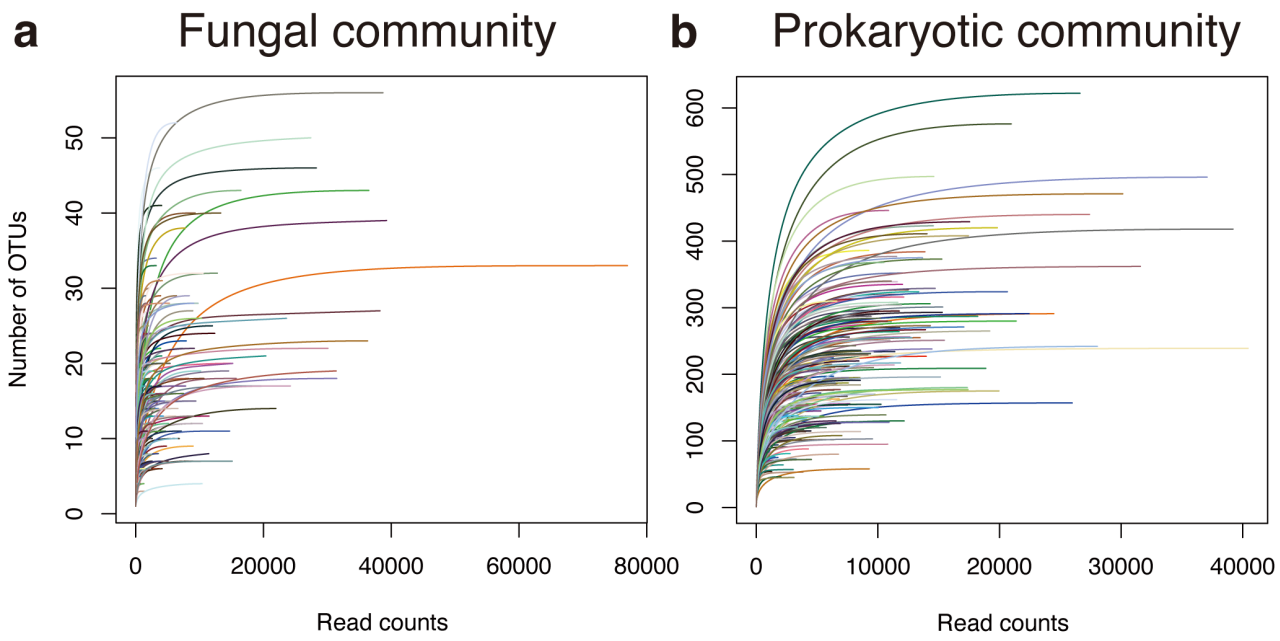

Supplementary Fig. S4 | Rarefaction curves. (**a**) Number of fungal OTUs detected in root samples. For visualization, the relationships between the number of sequencing reads and the number of fungal OTUs detected in 200 randomly selected samples are shown. (b) Number of prokaryotic OTUs.

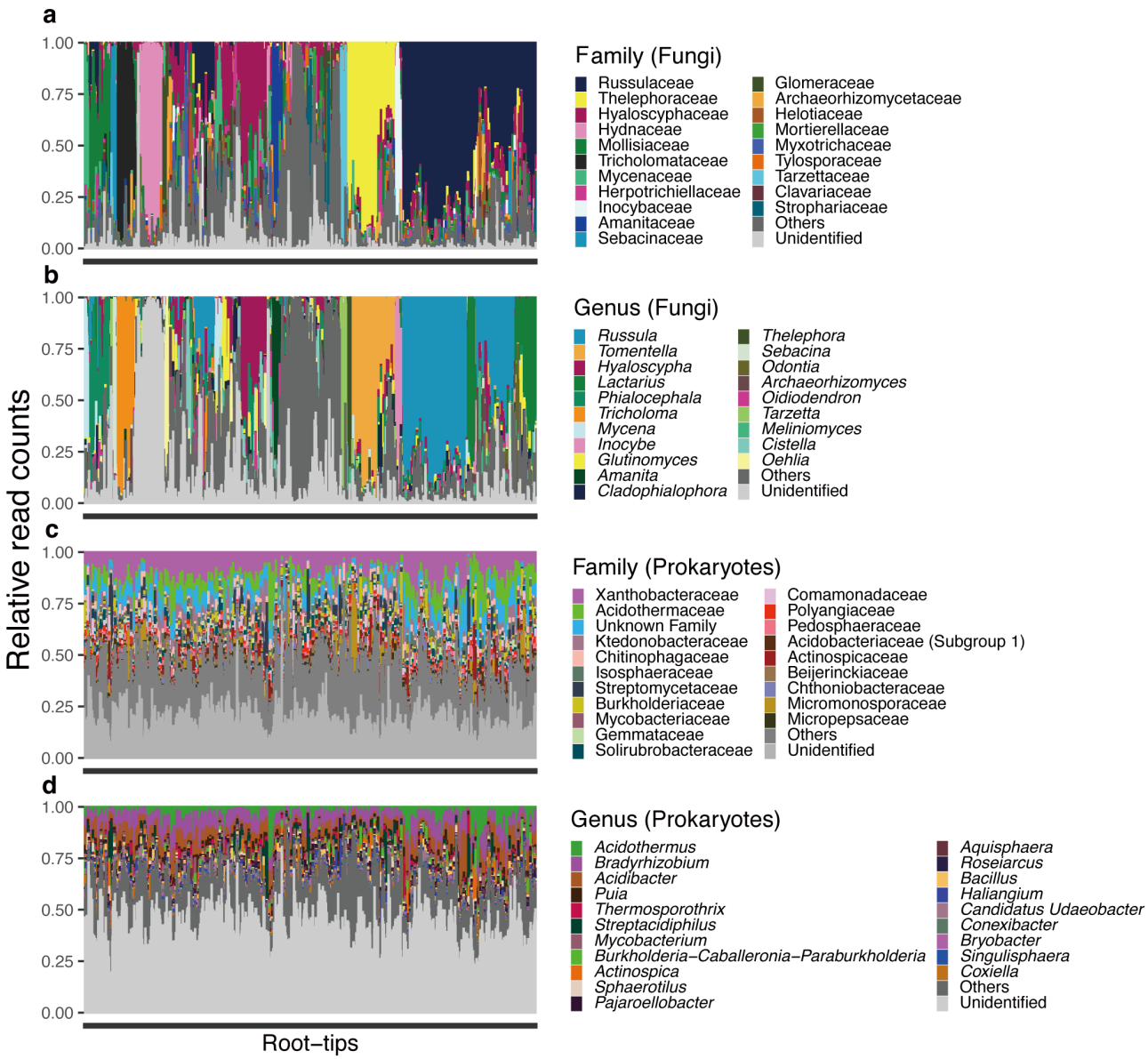

Supplementary Fig. S5 | Fungal and prokaryotic community compositions. (**a**) Family-level taxonomic compositions of fungal communities across 1,270 root-tip samples. (**b**) Genus-level taxonomic compositions of fungal communities. (**c**) Family-level taxonomic compositions of prokaryotic communities. (**d**) Genus-level taxonomic compositions of prokaryotic communities.

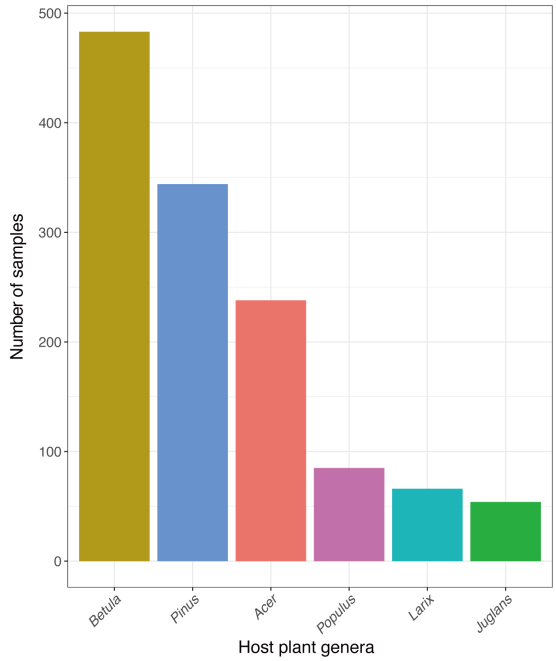

Supplementary Fig. S6 | Number of the samples from each host plant. The sample size of each host plant genera used in energy landscape analysis is shown. After a series of quality filtering, 1,270 root samples identified as those of major six plant genera (i.e., plant genera with more than 50 samples) were used in the statistical analysis.

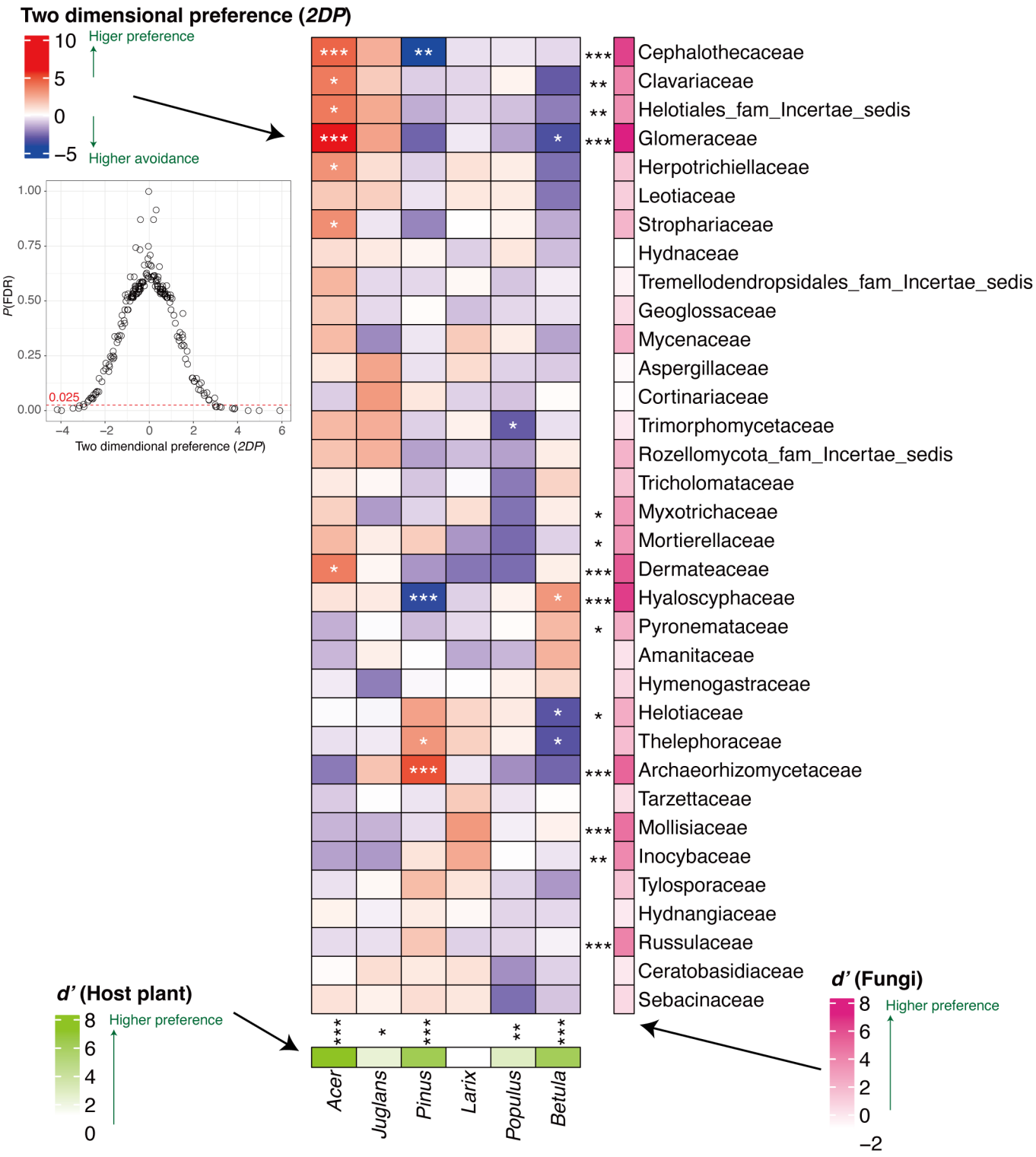
Two dimensional preference (2DP)
10
5
0
−5
Higer preference
Higher avoidance
1.00
0.75
0.50
0.25
0.00
P(FDR)
0.025
−4
−2
0
2
4
6
Two dimendional preference (2DP)
Cephalothecaceae
Clavariaceae
Helotiales_fam_Incertae_sedis
Glomeraceae
Herpotrichiellaceae
Leotiaceae
Strophariaceae
Hydnaceae
Tremellodendropsidales_fam_Incertae_sedis
Geoglossaceae
Mycenaceae
Aspergillaceae
Cortinariaceae
Trimorphomycetaceae
Rozellomycota_fam_Incertae_sedis
Tricholomataceae
Myxotrichaceae
Mortierellaceae
Dermateaceae
Hyaloscyphaceae
Pyronemataceae
Amanitaceae
Hymenogastraceae
Helotiaceae
Thelephoraceae
Archaeorhizomycetaceae
Tarzettaceae
Mollisiaceae
Inocybaceae
Tylosporaceae
Hydnangiaceae
Russulaceae
Ceratobasidiaceae
Sebacinaceae
Acer
Juglans
Pinus
Larix
Populus
Betula
d' (Host plant)
8
6
4
2
0
Higher preference
d' (Fungi)
8
6
4
2
0
−2
Higher preference

187

Supplementary Fig. S7 | Preferences in plant–fungus associations. Host preferences of the fungal families analyzed in the energy landscape analysis (rows) and symbiont preferences of the six host plant genera (column) are shown as *z*-standardized *d'* estimates. In addition, specificity of each host–symbiont pair is represented with a two-dimensional preference (*2DP*) estimate in the matrix heatmap, which indicates the extent to which the association of a target plant–fungal pair is observed more or less frequently than expected by chance. Significance of the *z*-standardized *d'* (one-tailed test) and *2DP* estimates (two-tailed test) are evaluated with the null model simulations (See Supplementary Methods; ***, $P\ (FDR) < 0.001$; **, $P\ (FDR) < 0.01$; *, $P\ (FDR) < 0.05$). The relationship between the *2DP* estimates and FDR-corrected *P* values are also shown in the left-side panel.

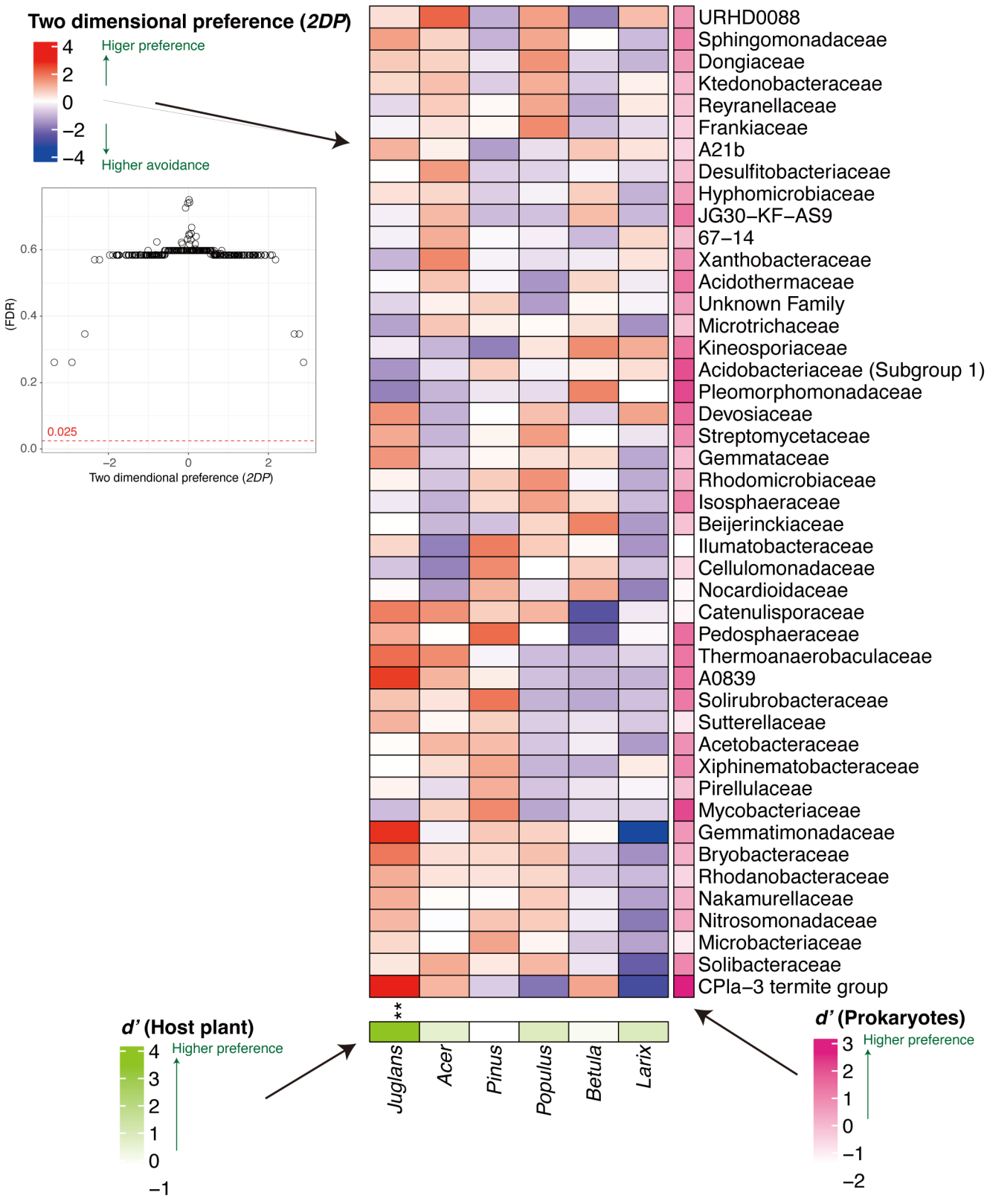

Supplementary Fig. S8 | Preferences in plant–prokaryote associations. Host preferences of the prokaryotic families analyzed in the energy landscape analysis (rows) and symbiont preferences of the six host plant genera (column) are shown with the *z*-standardized *d'* estimates. In addition, specificity of each host-symbiont pair is represented with a two-dimensional preference (*2DP*) estimate in the matrix heatmap, which indicates the extent to which the association of a target plant–prokaryote pair

is observed more or less frequently than expected by chance. Significance of the z-standardized *d'* (one-tailed test) and *2DP* estimates (two-tailed test) are evaluated with the null model simulations (See Supplementary Methods; ***, *P (FDR)* < 0.001; **, *P (FDR)* < 0.01; *, *P (FDR)* < 0.05). The relationship between the *2DP* estimates and FDR-corrected *P* values are also shown in the left-side panel.

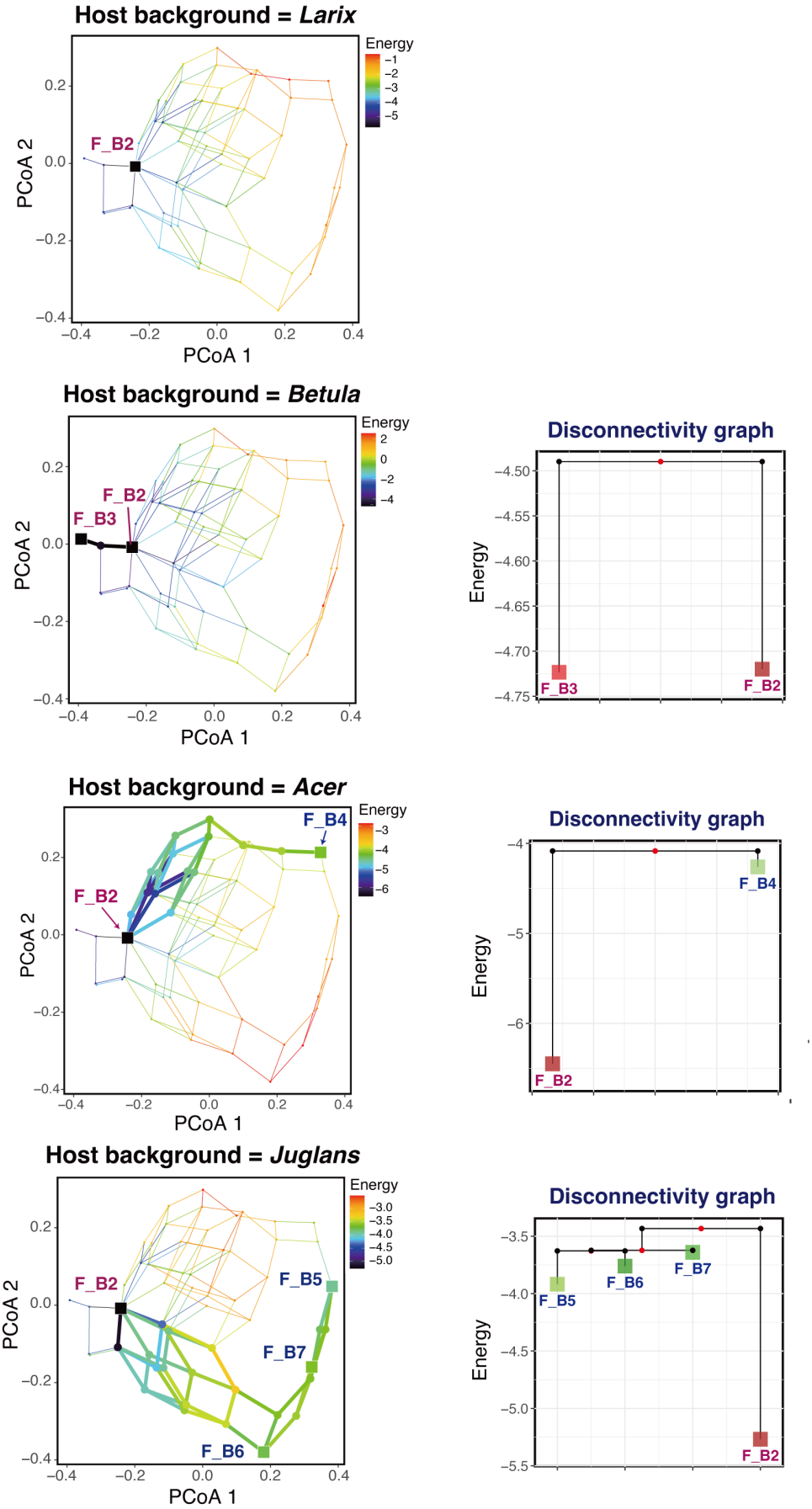

Supplementary Fig. S9 | Energy landscapes of the fungal community inferred by assuming *Larix, Betula, Acer* or *Juglans* host-plant backgrounds. The identity of host plants is included as an

explicit factor in the statistical model (Fig. 1b). We calculate energy of each community state and reconstructed energy-weighted assembly graph in each host-plant background. The basin bottoms (squares), the intermediate states (circles) and the lowest-energy transition pathways between them (thick lines) are visualized on the PCoA surface representing community states. Pathways and intermediates states for the basin bottoms inferred in other host-plant backgrounds are shown by thin lines and small circles, respectively. The "energy" of basin bottoms and boundary states between them is detailed in the "disconnectivity graphs".

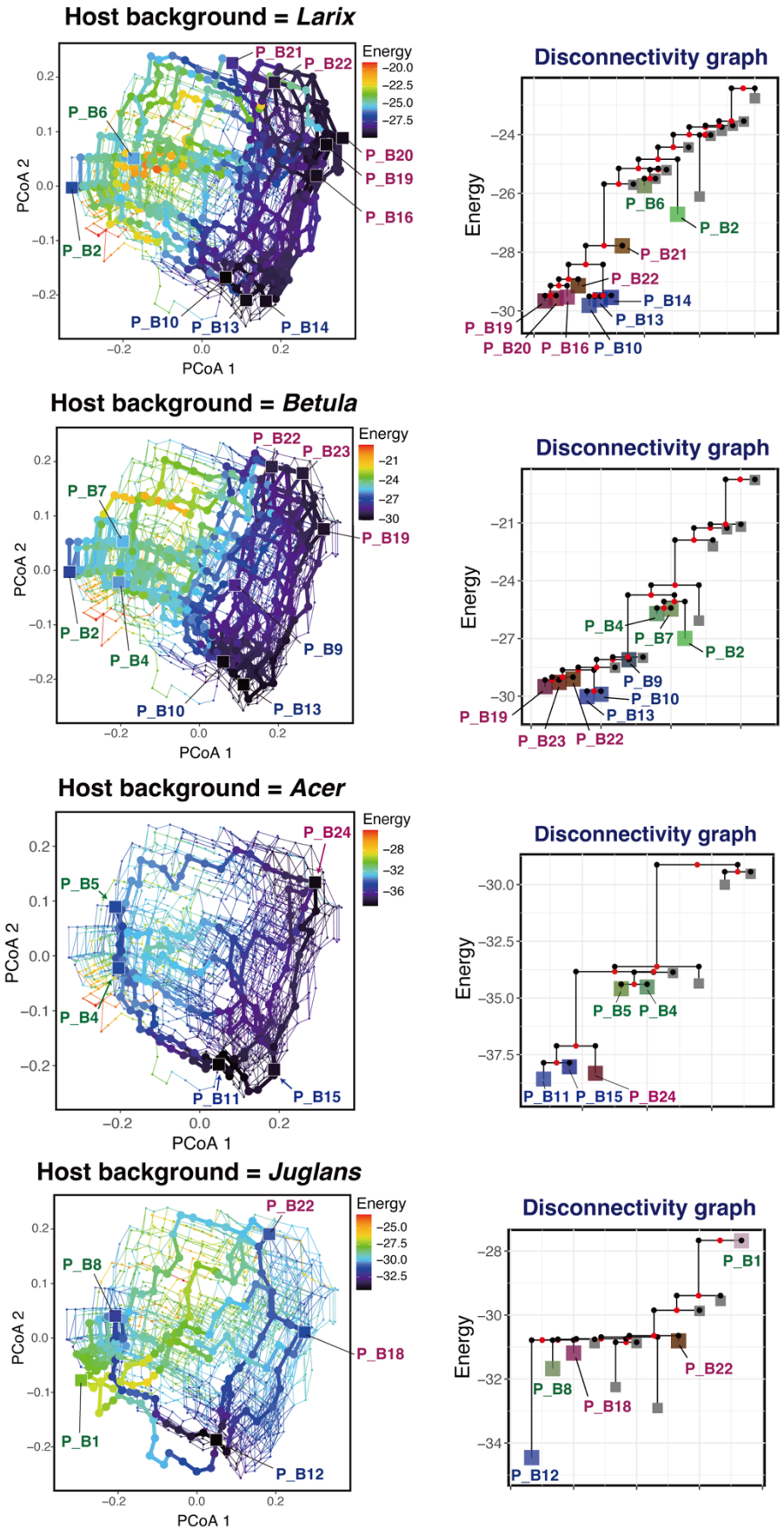

220

221 **Supplementary Fig. S10 | Energy landscapes of the prokaryotic community inferred by**
222 **assuming *Larix, Betula, Acer* or *Juglans* host-plant backgrounds.** The identity of host plants is

included as an explicit factor in the statistical model (Fig. 1b). We calculate energy of each community state and reconstructed energy-weighted assembly graph in each host-plant background. The basin bottoms (squares), the intermediate states (circles) and the lowest-energy transition pathways between them (thick lines) are visualized on the PCoA surface representing community states. Pathways and intermediates states for the basin bottoms inferred in other host-plant backgrounds are shown by thin lines and small circles, respectively. The "energy" of basin bottoms and boundary states between them is detailed in the "disconnectivity graphs".

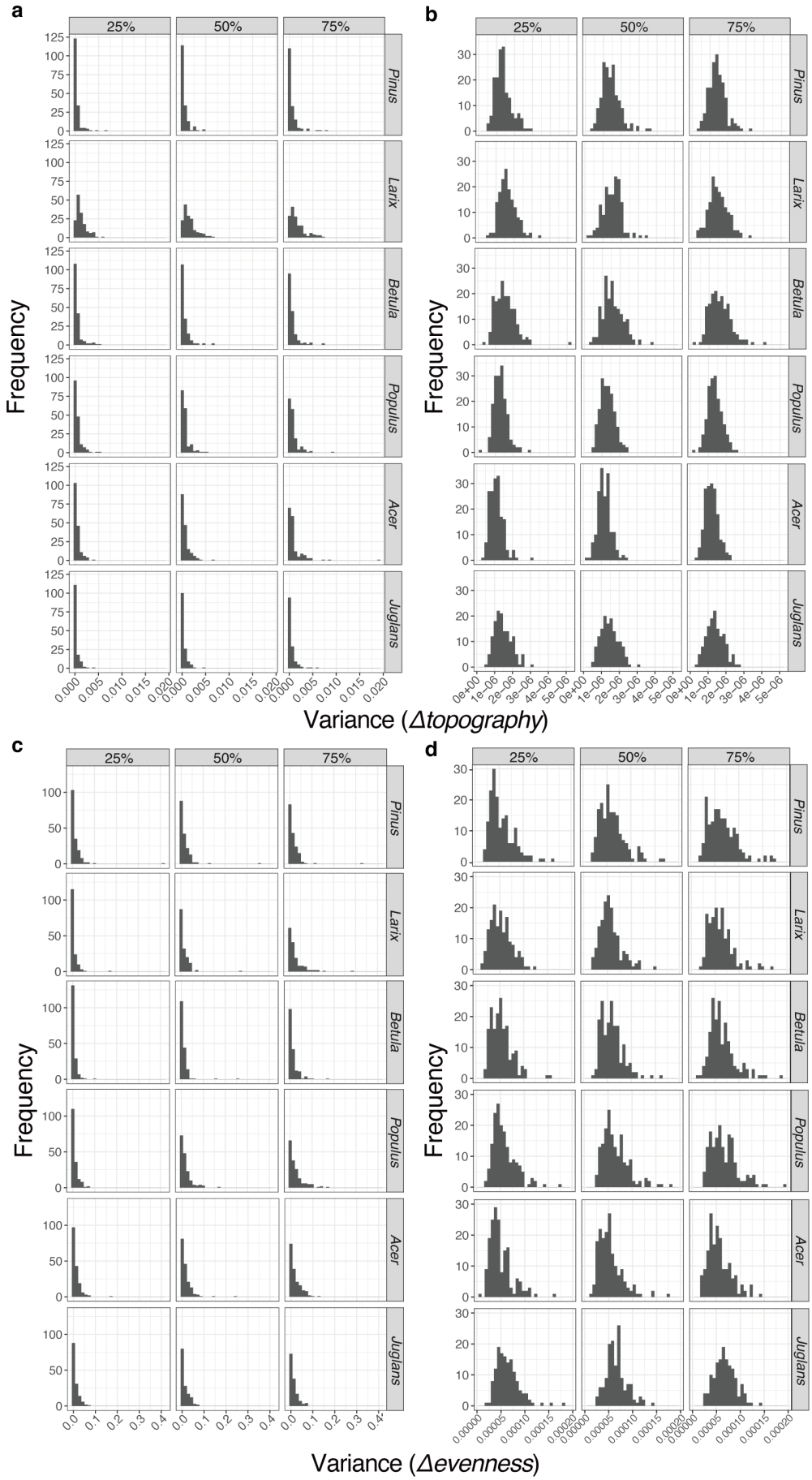

230

231 **Supplementary Fig. S11 | Histograms of the estimation variances in "keystoneness" metrices.**

The *Δtopography* and *Δevenness* values of each genus analyzed in Figure 4 were recalculated 30 times using different sets of 20,000 randomly initialized community states. Calculations were performed for each of the six host plants (rows), assuming different abundance quantile levels (columns; 25%, 50%, and 75% quantiles of relative read counts in samples in which the focal microbial taxon was present). (**a**) *Δtopography* for the fungal assembly landscape. (**b**) *Δtopography* for the prokaryotic assembly landscape. (**c**) *Δevenness* for the fungal assembly landscape. (**d**) *Δevenness* for the prokaryotic assembly landscape.

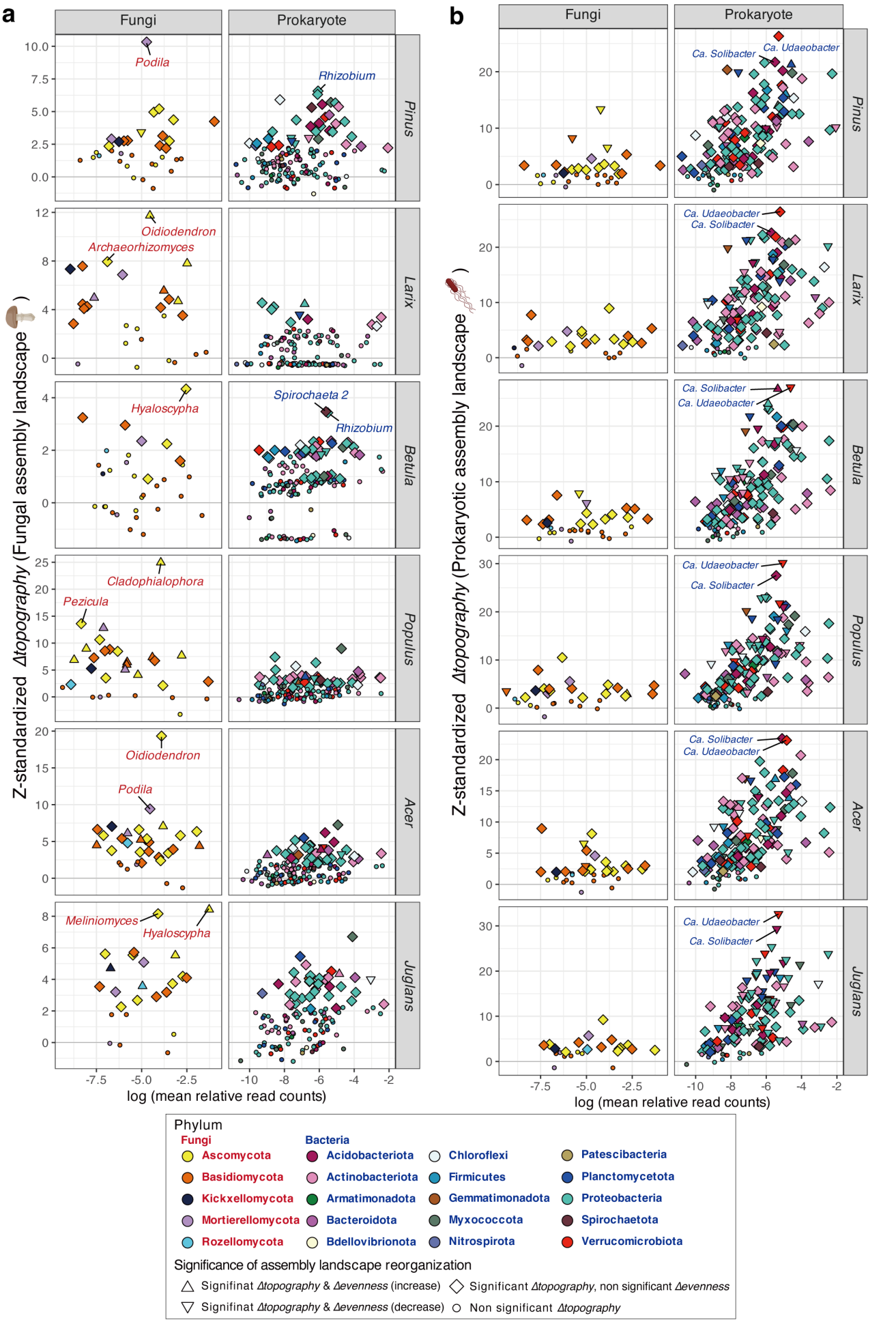
a
b
Fungi
Prokaryote
Pinus
Larix
Betula
Populus
Acer
Juglans
Podila
Rhizobium
Oidiodendron
Archaeorhizomyces
Hyaloscypha
Spirochaeta 2
Cladophialophora
Pezicula
Meliniomyces
Ca. Solibacter
Ca. Udaeobacter
Z-standardized Δtopography (Fungal assembly landscape)
Z-standardized Δtopography (Prokaryotic assembly landscape)
log (mean relative read counts)
Phylum
Fungi
Ascomycota
Basidiomycota
Kickxellomycota
Mortierellomycota
Rozellomycota
Bacteria
Acidobacteriota
Actinobacteriota
Armatimonadota
Bacteroidota
Bdellovibrionota
Chloroflexi
Firmicutes
Gemmatimonadota
Myxococcota
Nitrospirota
Patescibacteria
Planctomycetota
Proteobacteria
Spirochaetota
Verrucomicrobiota
Significance of assembly landscape reorganization
Signifinat Δtopography & Δevenness (increase)
Signifinat Δtopography & Δevenness (decrease)
Significant Δtopography, non significant Δevenness
Non significant Δtopography

Supplementary Fig. S12 | Potential impacts on the overall energy landscape architecture and the abundance of each microbial genus. (a) Z-standardized *Δtopography* of individual microbial genera in fungal energy landscapes. Genera whose abundance changes are inferred to substantially reshape the fungal community destinations within the energy landscape are highlighted in each host-plant background. The effects of fungal and prokaryotic genera are presented separately (left-side panels: fungal genera, right-side panels: prokaryotic genera). (b) Z-standardized *Δtopography* of individual microbial genera in prokaryotic energy landscapes.

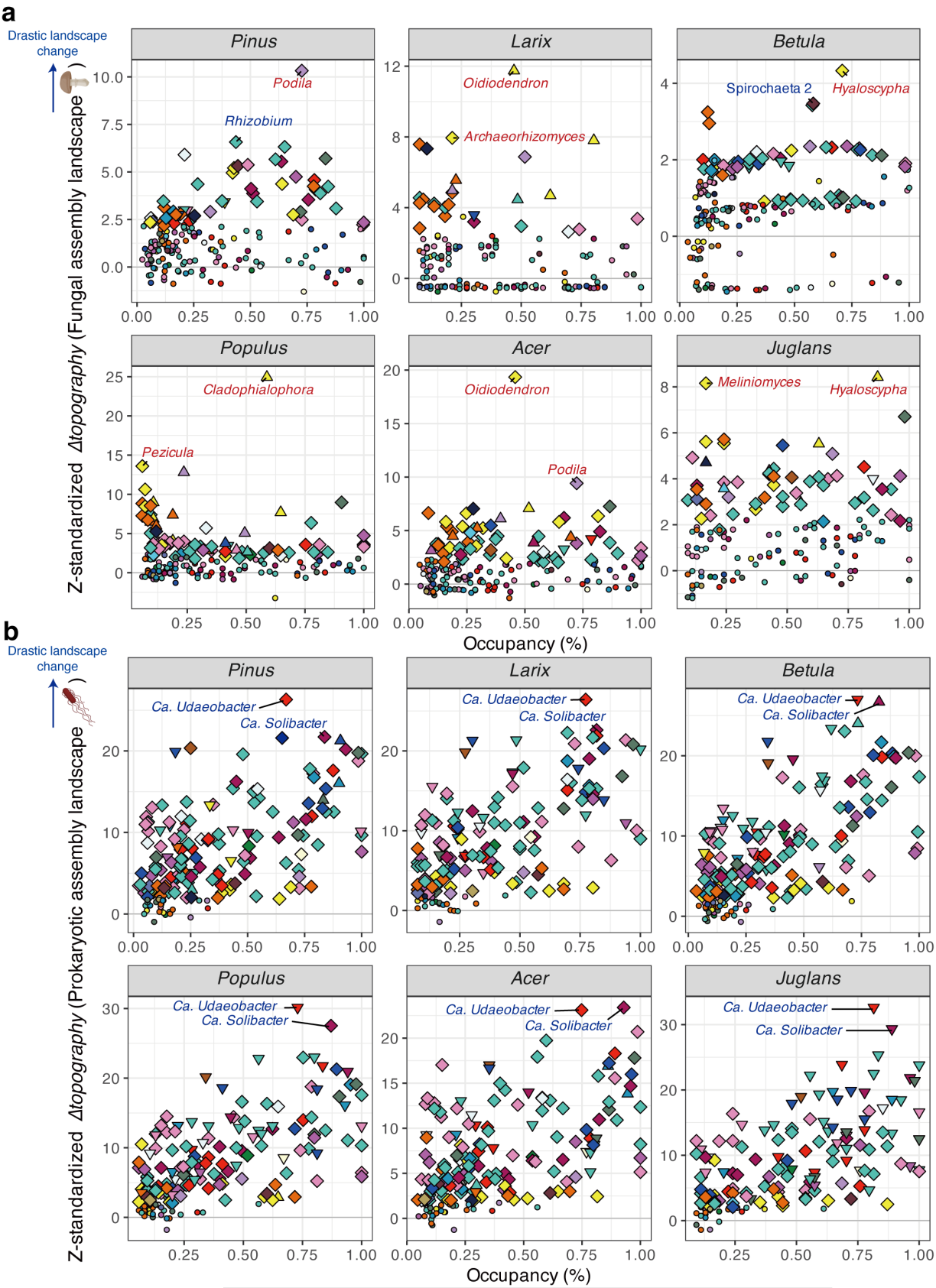
a
Drastic landscape change
Z-standardized Δtopography (Fungal assembly landscape)
Pinus
Podila
Rhizobium
Larix
Oidiodendron
Archaeorhizomyces
Betula
Spirochaeta 2
Hyaloscypha
Populus
Cladophialophora
Pezicula
Acer
Oidiodendron
Podila
Juglans
Meliniomyces
Hyaloscypha
Occupancy (%)
b
Drastic landscape change
Z-standardized Δtopography (Prokaryotic assembly landscape)
Pinus
Ca. Udaeobacter
Ca. Solibacter
Larix
Ca. Udaeobacter
Ca. Solibacter
Betula
Ca. Udaeobacter
Ca. Solibacter
Populus
Ca. Udaeobacter
Ca. Solibacter
Acer
Ca. Udaeobacter
Ca. Solibacter
Juglans
Ca. Udaeobacter
Ca. Solibacter
Occupancy (%)
Phylum
Fungi
Ascomycota
Basidiomycota
Kickxellomycota
Mortierellomycota
Rozellomycota
Bacteria
Acidobacteriota
Actinobacteriota
Armatimonadota
Bacteroidota
Bdellovibrionota
Chloroflexi
Firmicutes
Gemmatimonadota
Myxococcota
Nitrospirota
Patescibacteria
Planctomycetota
Proteobacteria
Spirochaetota
Verrucomicrobiota
Significance of assembly landscape reorganization
Signifinat Δtopography & Δevenness (increase)
Significant Δtopography, non significant Δevenness
Signifinat Δtopography & Δevenness (decrease)
Non significant Δtopography

Supplementary Fig. S13 | Potential impacts on the overall energy landscape architecture and the occupancy of each microbial genus. (**a**) Z-standardized *Δtopography* of individual microbial genera in fungal energy landscapes. Genera whose abundance changes are inferred to substantially reshape the fungal community destinations within the energy landscape are highlighted in each host plant background. (**b**) Z-standardized *Δtopography* of individual microbial genera in prokaryotic energy landscapes.

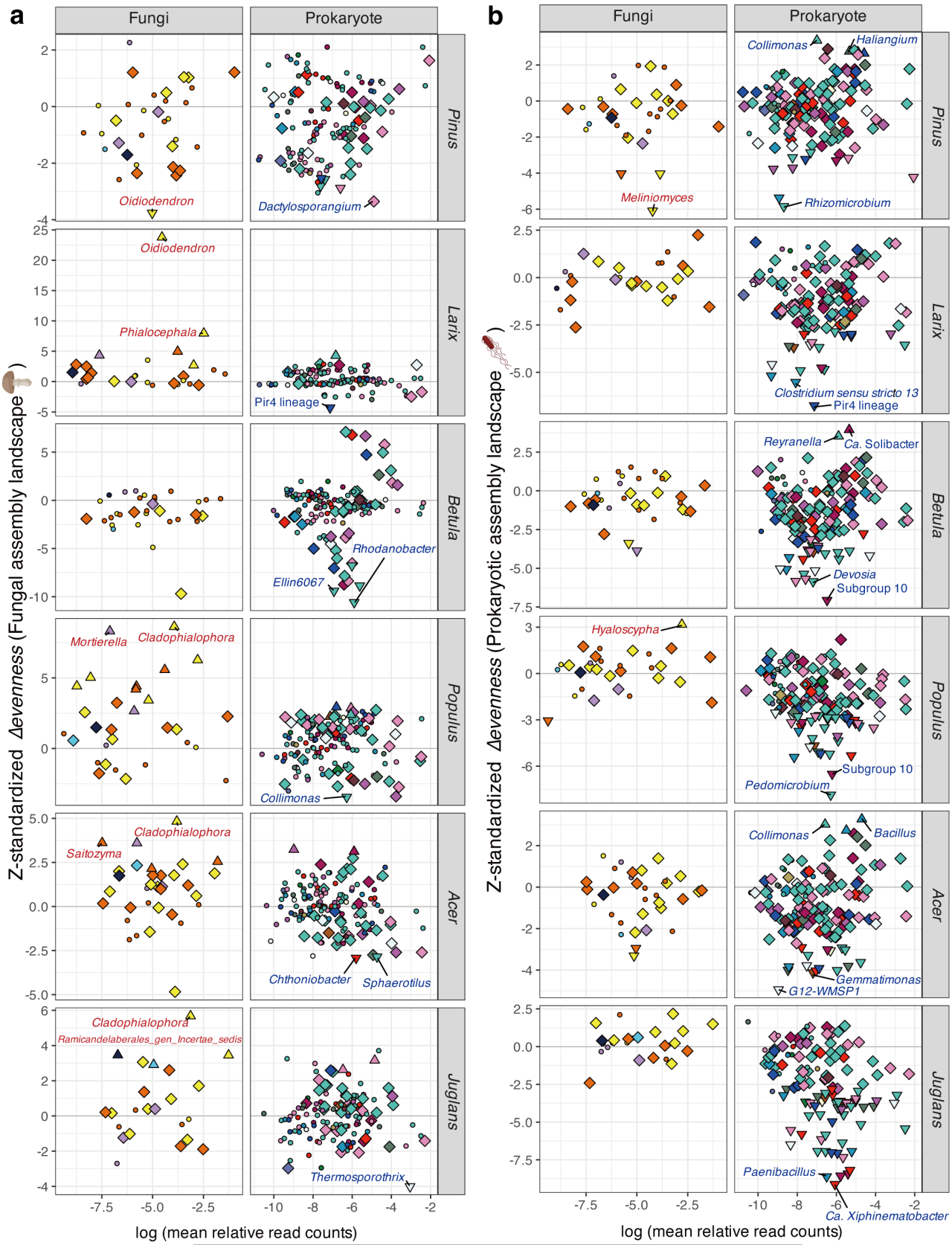
a
b
Fungi
Prokaryote
Pinus
Larix
Betula
Populus
Acer
Juglans
Z-standardized Δevenness (Fungal assembly landscape)
Z-standardized Δevenness (Prokaryotic assembly landscape)
log (mean relative read counts)
Oidiodendron
Dactylosporangium
Phialocephala
Pir4 lineage
Rhodanobacter
Ellin6067
Mortierella
Cladophialophora
Collimonas
Saitozyma
Chthoniobacter
Sphaerotilus
Ramicandelaberales_gen_Incertae_sedis
Thermosporothrix
Meliniomyces
Haliangium
Rhizomicrobium
Clostridium sensu stricto 13
Reyranella
Ca. Solibacter
Devosia
Subgroup 10
Hyaloscypha
Pedomicrobium
Bacillus
Gemmatimonas
G12-WMSP1
Paenibacillus
Ca. Xiphinematobacter
Phylum
Fungi
Ascomycota
Basidiomycota
Kickxellomycota
Mortierellomycota
Rozellomycota
Bacteria
Acidobacteriota
Actinobacteriota
Armatimonadota
Bacteroidota
Bdellovibrionota
Chloroflexi
Firmicutes
Gemmatimonadota
Myxococcota
Nitrospirota
Patescibacteria
Planctomycetota
Proteobacteria
Spirochaetota
Verrucomicrobiota
Significance of assembly landscape reorganization
Signifinat Δtopography & Δevenness (increase)
Signifinat Δtopography & Δevenness (decrease)
Significant Δtopography, non significant Δevenness
Non significant Δtopography

Supplementary Fig. S14 | Potential impacts on the evenness of the basin distributions and the relative abundance of each microbial genus. (**a**) Z-standardized *Δevenness* of individual microbial genera in fungal energy landscapes. Genera whose abundance changes are inferred to substantially alter the basin distributions and frequencies within the energy landscape are highlighted in each host plant background. The effects of fungal and prokaryotic genera are presented separately (left-side panels: fungal genera, right-side panels: prokaryotic genera). (**b**) Z-standardized *Δevenness* of individual microbial genera in prokaryotic energy landscapes.

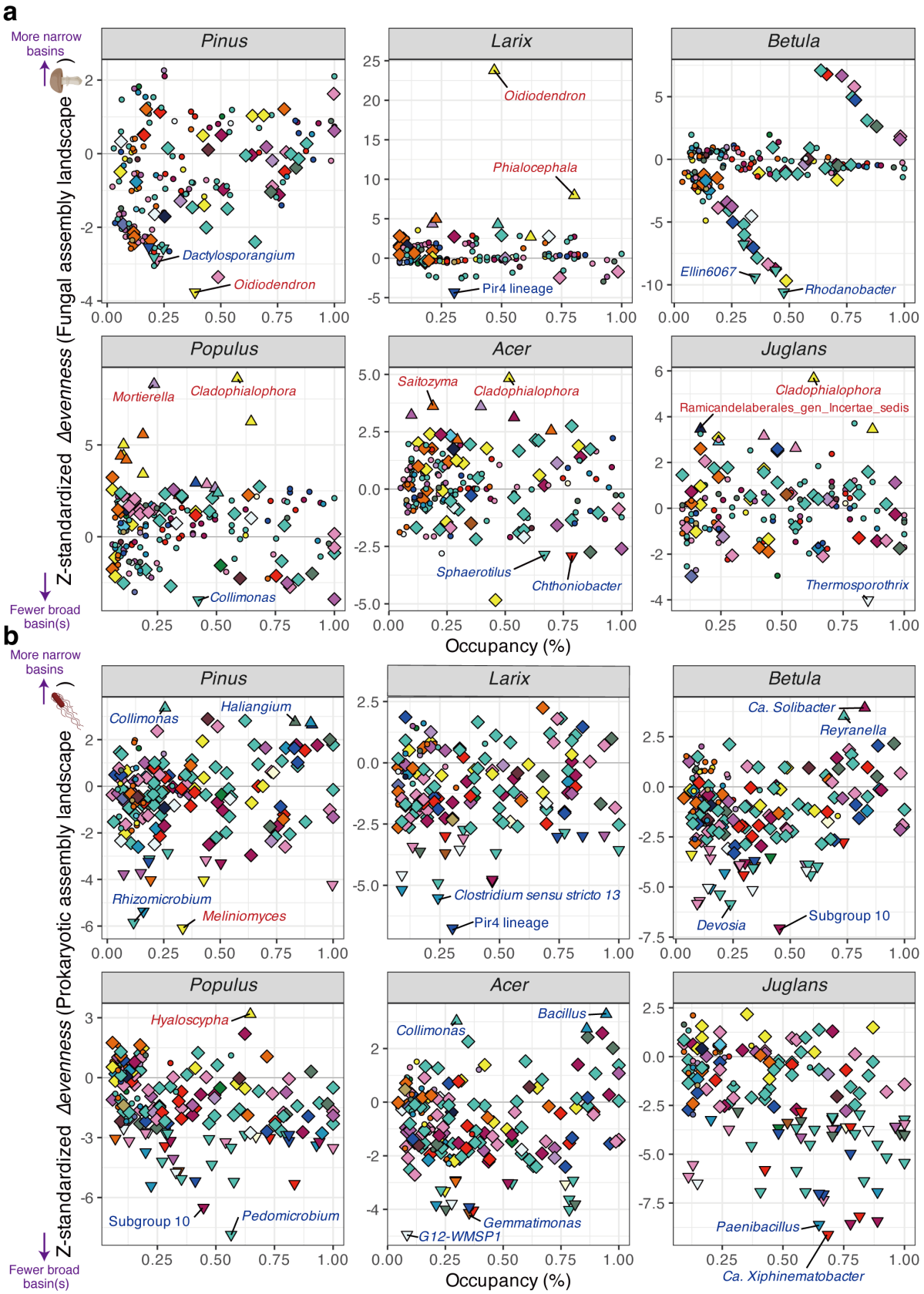
a
More narrow basins
Fewer broad basin(s)
Z-standardized Δevenness (Fungal assembly landscape)
Pinus
Larix
Betula
Populus
Acer
Juglans
Dactylosporangium
Oidiodendron
Oidiodendron
Phialocephala
Pir4 lineage
Ellin6067
Rhodanobacter
Mortierella
Cladophialophora
Collimonas
Saitozyma
Cladophialophora
Sphaerotilus
Chthoniobacter
Cladophialophora
Ramicandelaberales_gen_Incertae_sedis
Thermosporothrix
b
More narrow basins
Fewer broad basin(s)
Z-standardized Δevenness (Prokaryotic assembly landscape)
Pinus
Larix
Betula
Populus
Acer
Juglans
Collimonas
Haliangium
Rhizomicrobium
Meliniomyces
Clostridium sensu stricto 13
Pir4 lineage
Ca. Solibacter
Reyranella
Devosia
Subgroup 10
Hyaloscypha
Subgroup 10
Pedomicrobium
Bacillus
Collimonas
Gemmatimonas
G12-WMSP1
Paenibacillus
Ca. Xiphinematobacter
Occupancy (%)
Occupancy (%)
Phylum
Fungi
Ascomycota
Basidiomycota
Kickxellomycota
Mortierellomycota
Rozellomycota
Bacteria
Acidobacteriota
Actinobacteriota
Armatimonadota
Bacteroidota
Bdellovibrionota
Chloroflexi
Firmicutes
Gemmatimonadota
Myxococcota
Nitrospirota
Patescibacteria
Planctomycetota
Proteobacteria
Spirochaetota
Verrucomicrobiota
Significance of assembly landscape reorganization
Signifinat Δtopography & Δevenness (increase)
Significant Δtopography, non significant Δevenness
Signifinat Δtopography & Δevenness (decrease)
Non significant Δtopography

265

Supplementary Fig. S15 | Potential impacts on the evenness of the basin distributions and the occupancy of each microbial genus. (**a**) Z-standardized *Δevenness* of individual microbial genera in fungal energy landscapes. Genera whose abundance changes are inferred to substantially alter the basin distributions and frequencies within the energy landscape are highlighted in each host plant background. (**b**) Z-standardized *Δevenness* of individual microbial genera in prokaryotic energy landscapes.

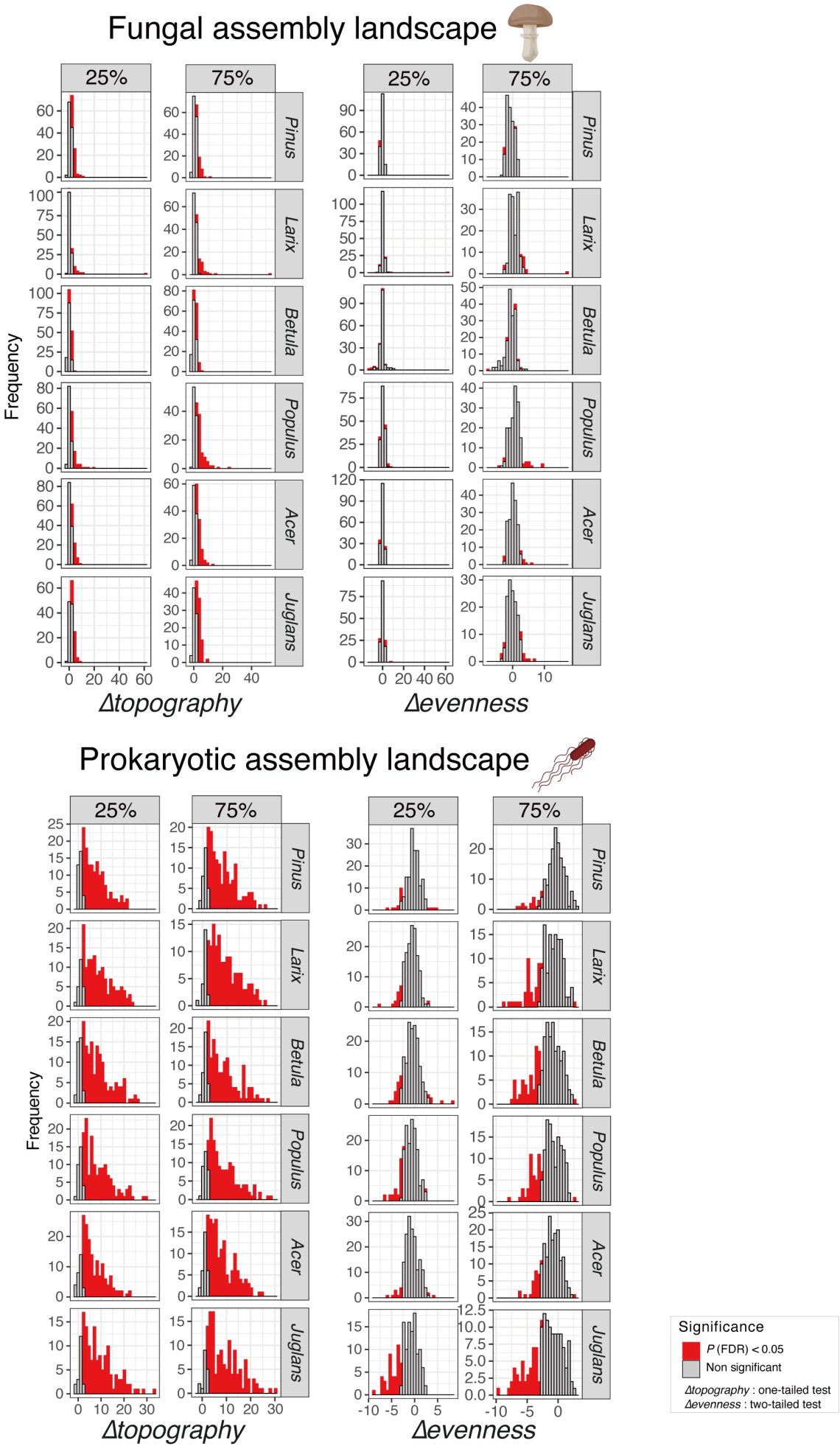
Fungal assembly landscape
25%
75%
25%
75%
Pinus
Larix
Betula
Populus
Acer
Juglans
Frequency
Δtopography
Δevenness
Prokaryotic assembly landscape
25%
75%
25%
75%
Pinus
Larix
Betula
Populus
Acer
Juglans
Frequency
Δtopography
Δevenness
Significance
P (FDR) < 0.05
Non significant
Δtopography : one-tailed test
Δevenness : two-tailed test

Supplementary Fig. S16 | Histograms of "keystoneness" metrics based on 25% and 75% quantiles of the relative abundances of each microbial genus. The z-standardized *Δtopography* and *Δevenness* metrics respectively represent changes in the overall topography and evenness of basin distributions in fungal and prokaryotic energy landscape architecture along the two abundance gradients of a focal genus (see Fig. 1d-g). Results are shown separately for each host-plant background.

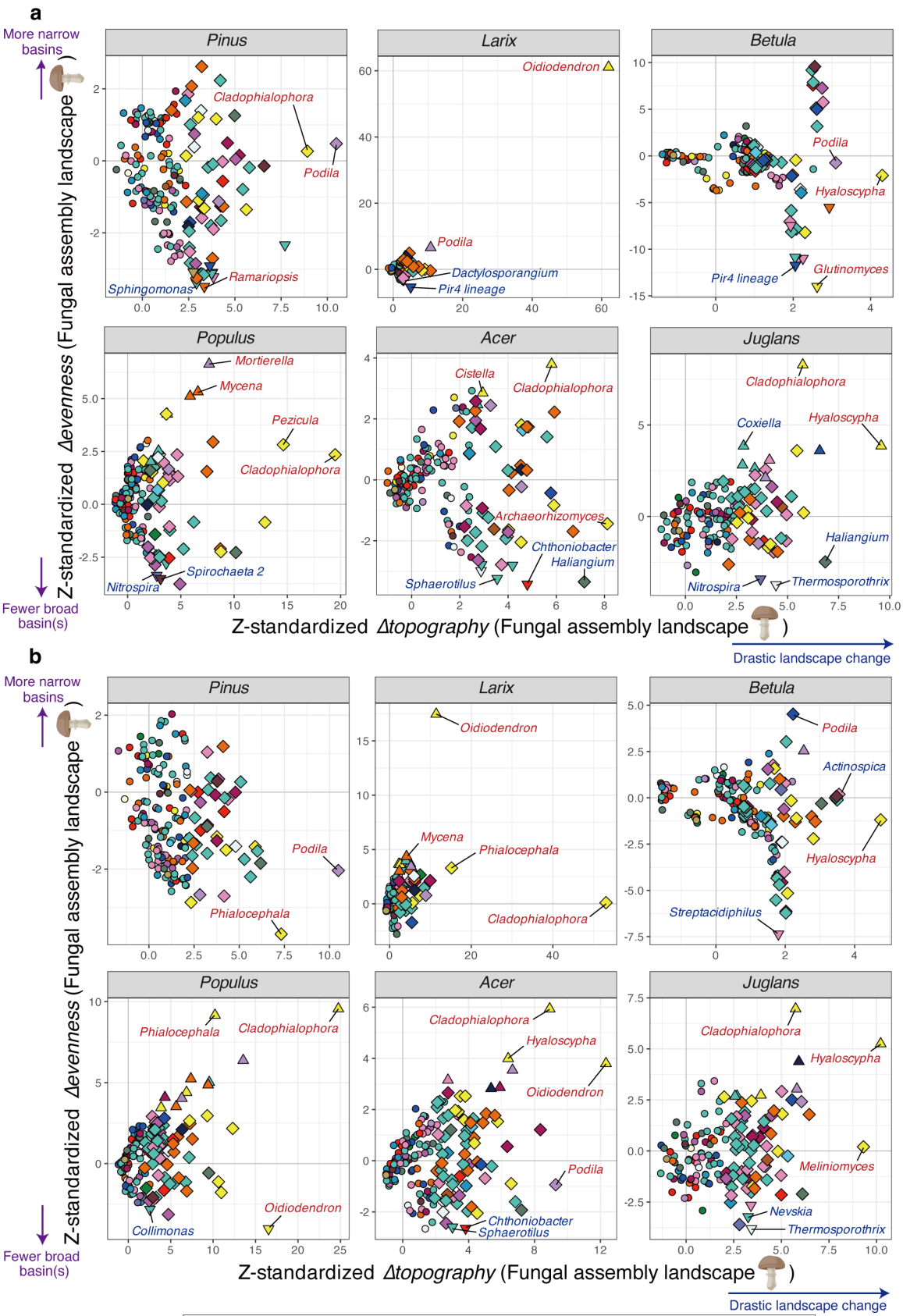
a
More narrow basins
Fewer broad basin(s)
Z-standardized Δevenness (Fungal assembly landscape)
Pinus
Cladophialophora
Podila
Sphingomonas
Ramariopsis
Larix
Oidiodendron
Podila
Dactylosporangium
Pir4 lineage
Betula
Podila
Hyaloscypha
Pir4 lineage
Glutinomyces
Populus
Mortierella
Mycena
Pezicula
Cladophialophora
Nitrospira
Spirochaeta 2
Acer
Cistella
Cladophialophora
Archaeorhizomyces
Chthoniobacter
Haliangium
Sphaerotilus
Juglans
Cladophialophora
Coxiella
Hyaloscypha
Haliangium
Nitrospira
Thermosporothrix
Z-standardized Δtopography (Fungal assembly landscape)
Drastic landscape change
b
More narrow basins
Fewer broad basin(s)
Z-standardized Δevenness (Fungal assembly landscape)
Pinus
Podila
Phialocephala
Larix
Oidiodendron
Mycena
Phialocephala
Cladophialophora
Betula
Podila
Actinospica
Hyaloscypha
Streptacidiphilus
Populus
Phialocephala
Cladophialophora
Collimonas
Oidiodendron
Acer
Cladophialophora
Hyaloscypha
Oidiodendron
Podila
Chthoniobacter
Sphaerotilus
Juglans
Cladophialophora
Hyaloscypha
Meliniomyces
Nevskia
Thermosporothrix
Z-standardized Δtopography (Fungal assembly landscape)
Drastic landscape change
Phylum
Fungi
Ascomycota
Basidiomycota
Kickxellomycota
Mortierellomycota
Rozellomycota
Bacteria
Acidobacteriota
Actinobacteriota
Armatimonadota
Bacteroidota
Bdellovibrionota
Chloroflexi
Firmicutes
Gemmatimonadota
Myxococcota
Nitrospirota
Patescibacteria
Planctomycetota
Proteobacteria
Spirochaetota
Verrucomicrobiota
Significance of assembly landscape reorganization
Signifinat Δtopography & Δevenness (increase)
Significant Δtopography, non significant Δevenness
Signifinat Δtopography & Δevenness (decrease)
Non significant Δtopography

Supplementary Fig. S17 | Potential impacts on the fungal community assembly along the two representative abundance gradients of each microbial genus. (**a**) Taxa strongly associated with the energy landscape reorganizations along their abundance gradients from 0% (absence) to 25% quantile. On two-dimensional planes defined by *Δtopography* and *Δevenness*, microbial genera whose abundance changes were inferred to substantially reshape the energy landscape architecture of root-associated fungal communities are highlighted. (**b**) Taxa strongly associated with the energy landscape reorganizations along their abundance gradients from 0% (absence) to 75% quantile.

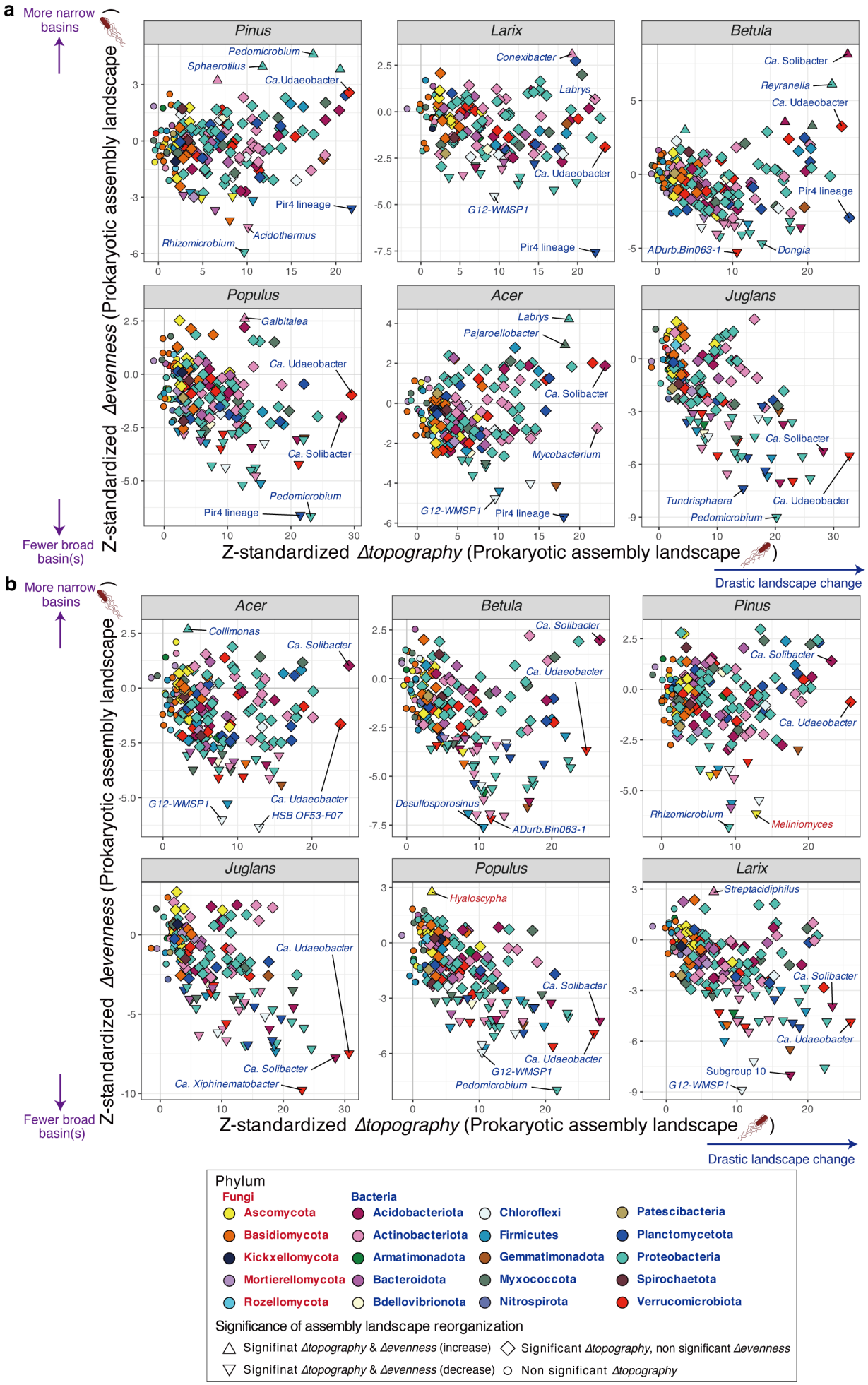
a
More narrow basins
Fewer broad basin(s)
Z-standardized Δevenness (Prokaryotic assembly landscape)
Pinus
Pedomicrobium
Sphaerotilus
Ca.Udaeobacter
Pir4 lineage
Acidothermus
Rhizomicrobium
Larix
Conexibacter
Labrys
Ca. Udaeobacter
G12-WMSP1
Pir4 lineage
Betula
Ca. Solibacter
Reyranella
Ca. Udaeobacter
Pir4 lineage
ADurb.Bin063-1
Dongia
Populus
Galbitalea
Ca. Udaeobacter
Ca. Solibacter
Pedomicrobium
Pir4 lineage
Acer
Labrys
Pajaroellobacter
Ca. Solibacter
Mycobacterium
G12-WMSP1
Pir4 lineage
Juglans
Ca. Solibacter
Tundrisphaera
Ca. Udaeobacter
Pedomicrobium
Z-standardized Δtopography (Prokaryotic assembly landscape)
Drastic landscape change
b
More narrow basins
Fewer broad basin(s)
Z-standardized Δevenness (Prokaryotic assembly landscape)
Acer
Collimonas
Ca. Solibacter
Ca. Udaeobacter
G12-WMSP1
HSB OF53-F07
Betula
Ca. Solibacter
Ca. Udaeobacter
Desulfosporosinus
ADurb.Bin063-1
Pinus
Ca. Solibacter
Ca. Udaeobacter
Rhizomicrobium
Meliniomyces
Juglans
Ca. Udaeobacter
Ca. Solibacter
Ca. Xiphinematobacter
Populus
Hyaloscypha
Ca. Solibacter
Ca. Udaeobacter
G12-WMSP1
Pedomicrobium
Larix
Streptacidiphilus
Ca. Solibacter
Ca. Udaeobacter
Subgroup 10
G12-WMSP1
Z-standardized Δtopography (Prokaryotic assembly landscape)
Drastic landscape change
Phylum
Fungi
Ascomycota
Basidiomycota
Kickxellomycota
Mortierellomycota
Rozellomycota
Bacteria
Acidobacteriota
Actinobacteriota
Armatimonadota
Bacteroidota
Bdellovibrionota
Chloroflexi
Firmicutes
Gemmatimonadota
Myxococcota
Nitrospirota
Patescibacteria
Planctomycetota
Proteobacteria
Spirochaetota
Verrucomicrobiota
Significance of assembly landscape reorganization
Signifinat Δtopography & Δevenness (increase)
Significant Δtopography, non significant Δevenness
Signifinat Δtopography & Δevenness (decrease)
Non significant Δtopography

Supplementary Fig. S18 | Potential impacts on the prokaryotic community assembly along the two representative abundance gradients of each microbial genus. (**a**) Taxa strongly associated with the energy landscape reorganizations along their abundance gradients from 0% (absence) to 25% quantile. On two-dimensional planes defined by *Δtopography* and *Δevenness*, microbial genera whose abundance changes were inferred to substantially reshape the energy landscape architecture of root-associated prokaryotic communities are highlighted. (**b**) Taxa strongly associated with the energy landscape reorganizations along their abundance gradients from 0% (absence) to 75% quantile.

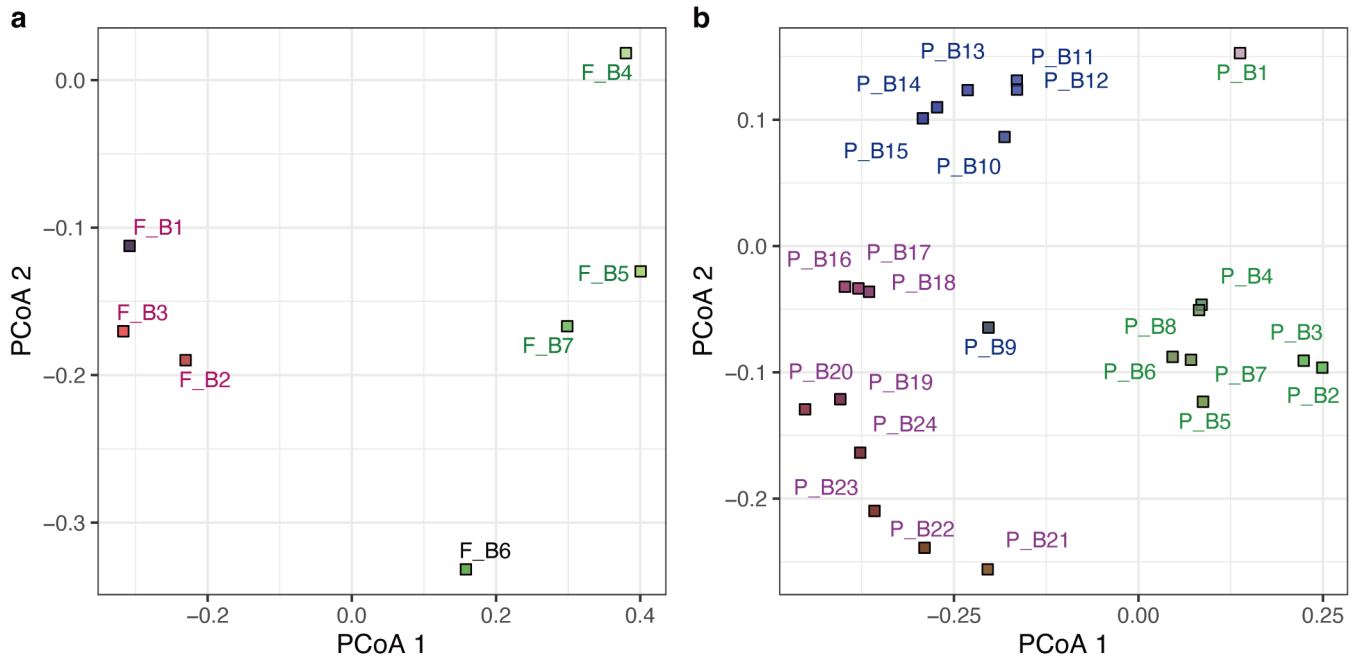

297

298 **Supplementary Fig. S19 | Community structures of the basin bottoms.** (**a**) Principal coordinate
299 analysis (PCoA) of the fungal basin bottoms shown in Figure 2c. Dissimilarities among the bottom
300 states are calculated based on Jaccard distance. The colors correspond to those in Figure 2c and
301 Supplementary Figure S20. (**b**) PCoA of the prokaryotic basin bottoms shown in Figure 3c. The colors
302 correspond to those in Figure 3c and Supplementary Figure S23.

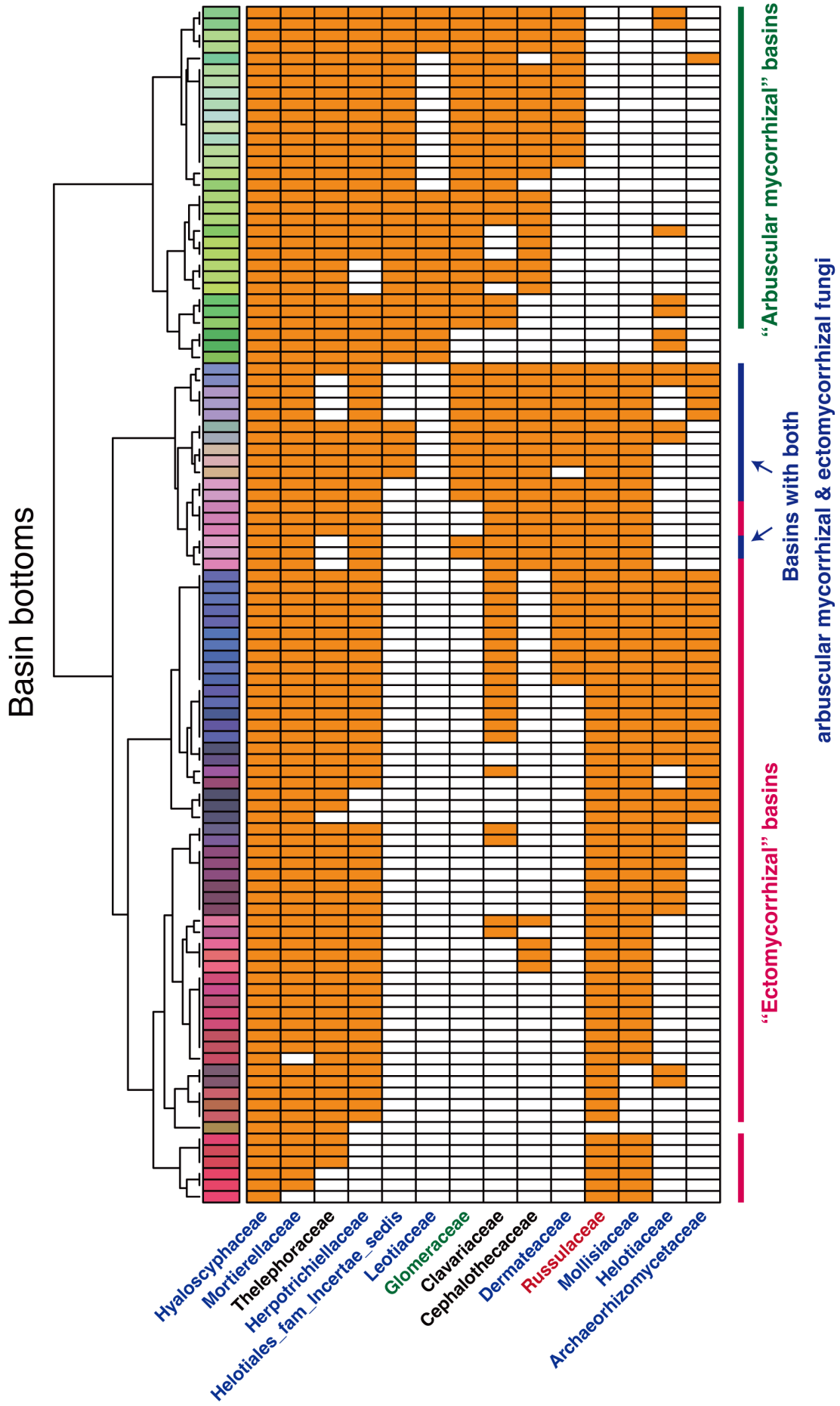

303

304 **Supplementary Fig. S20 | Community states at basin bottoms of fungal energy landscapes.** The

basin bottoms inferred across the six host-plant backgrounds in Figures 2c and 5 as well as in Supplementary Figures S21 and S22 are shown with a dendrogram representing taxonomic membership similarity. The color gradient of left-side panel represents the degree of similarity/dissimilarity among community states, corresponding to those illustrated in the flow diagrams (see Fig. 5 and Supplementary Figs. S21 and S22). Depending on the presence/absence of Glomeraceae and Russulaceae, "arbuscular mycorrhizal" and "ectomycorrhizal" basins are tentatively defined. In addition to the basins in Figures 2c, some basins including both Glomeraceae and Russulaceae were detected. Fungal families are colored according to functional guilds: green, arbuscular mycorrhizal; red, ectomycorrhizal; blue, potentially endophytic; black, families with multiple or other functions.

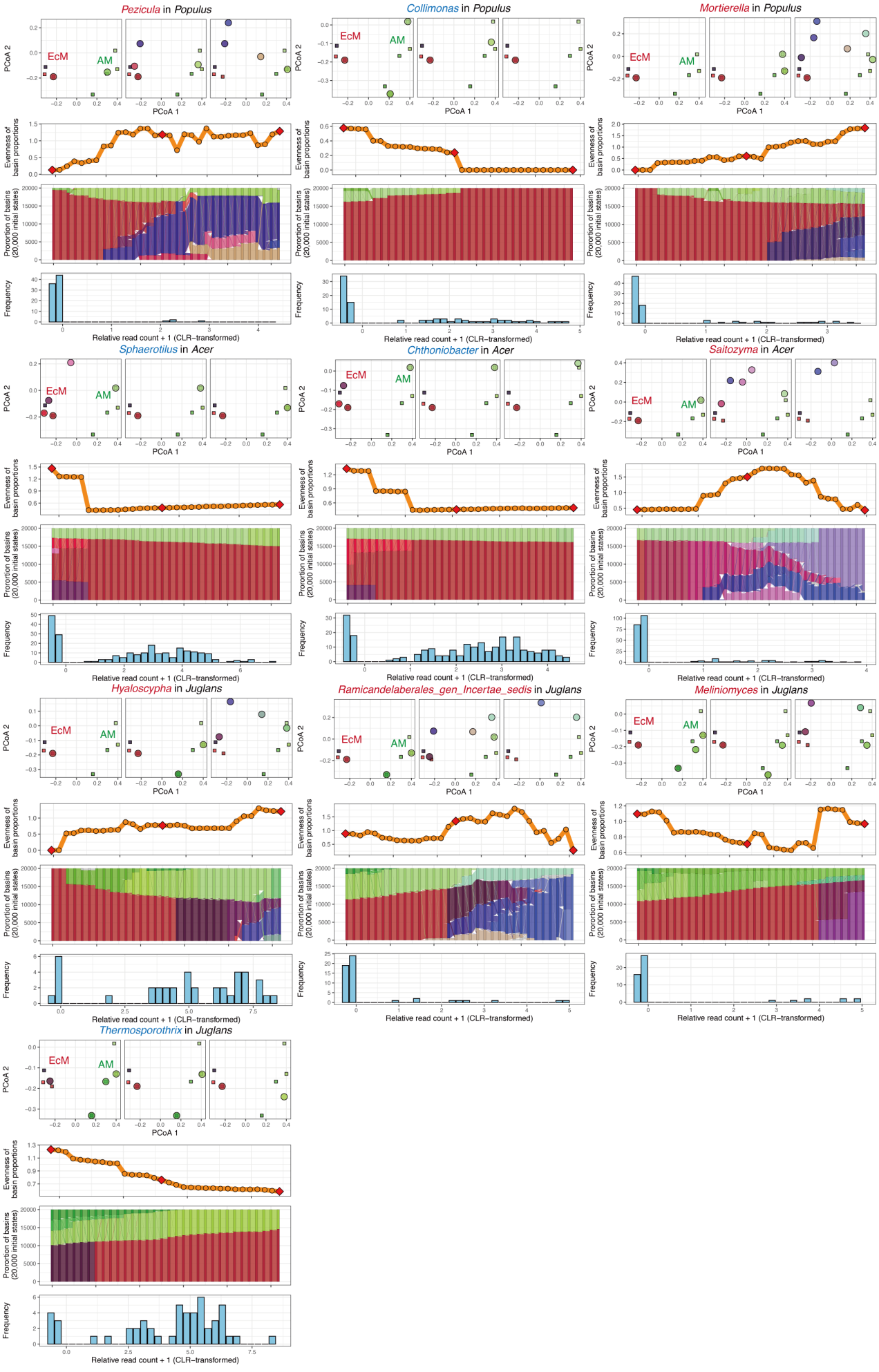
Pezicula in Populus
Collimonas in Populus
Mortierella in Populus
Sphaerotilus in Acer
Chthoniobacter in Acer
Saitozyma in Acer
Hyaloscypha in Juglans
Ramicandelaberales_gen_Incertae_sedis in Juglans
Meliniomyces in Juglans
Thermosporothrix in Juglans
EcM
AM
PCoA 1
PCoA 2
Evenness of basin proportions
Prorortion of basins (20,000 initial states)
Frequency
Relative read count + 1 (CLR−transformed)

Supplementary Fig. S21 | Fungal energy landscape reorganization in the dual mycorrhizal host-plant backgrounds. Along the abundance gradient of each microbial genus highlighted in Figure 4b (*Populus*, *Acer* and *Juglans*), changes in the frequency distribution of fungal energy landscape basins are shown. Frequencies are evaluated through 20,000 simulations of community assemblies from randomly generated initial states, under 32 abundance conditions ranging from absence to the maximum observed abundance in the host. On the PCoA planes, the basin bottoms detected at three representative abundance levels within 32 equally spaced relative abundance steps—absence (step 1), intermediate abundance (step 16), and maximum abundance (step 32)—are shown as circles, together with the states detected in Figure 2c (see Supplementary Fig. S19a). The Shannon entropy of the basin frequencies is also shown along the abundance axis (CLR-transformed relative read counts of a focal genus). In addition, the destinations of the initial communities in each condition of the focal genus's abundance are indicated in the flow diagrams with the histograms of their relative abundances in the hosts. Each bar plot depicts the frequency of basin bottoms detected under the corresponding abundance condition. The bottoms which the same initial community state converged across adjacent abundance conditions (steps) are connected with bands. Colors represent community compositional similarity based on Jaccard distance, with more similar compositions rendered in more similar colors (see Fig. 2c; Supplementary Fig. S20).

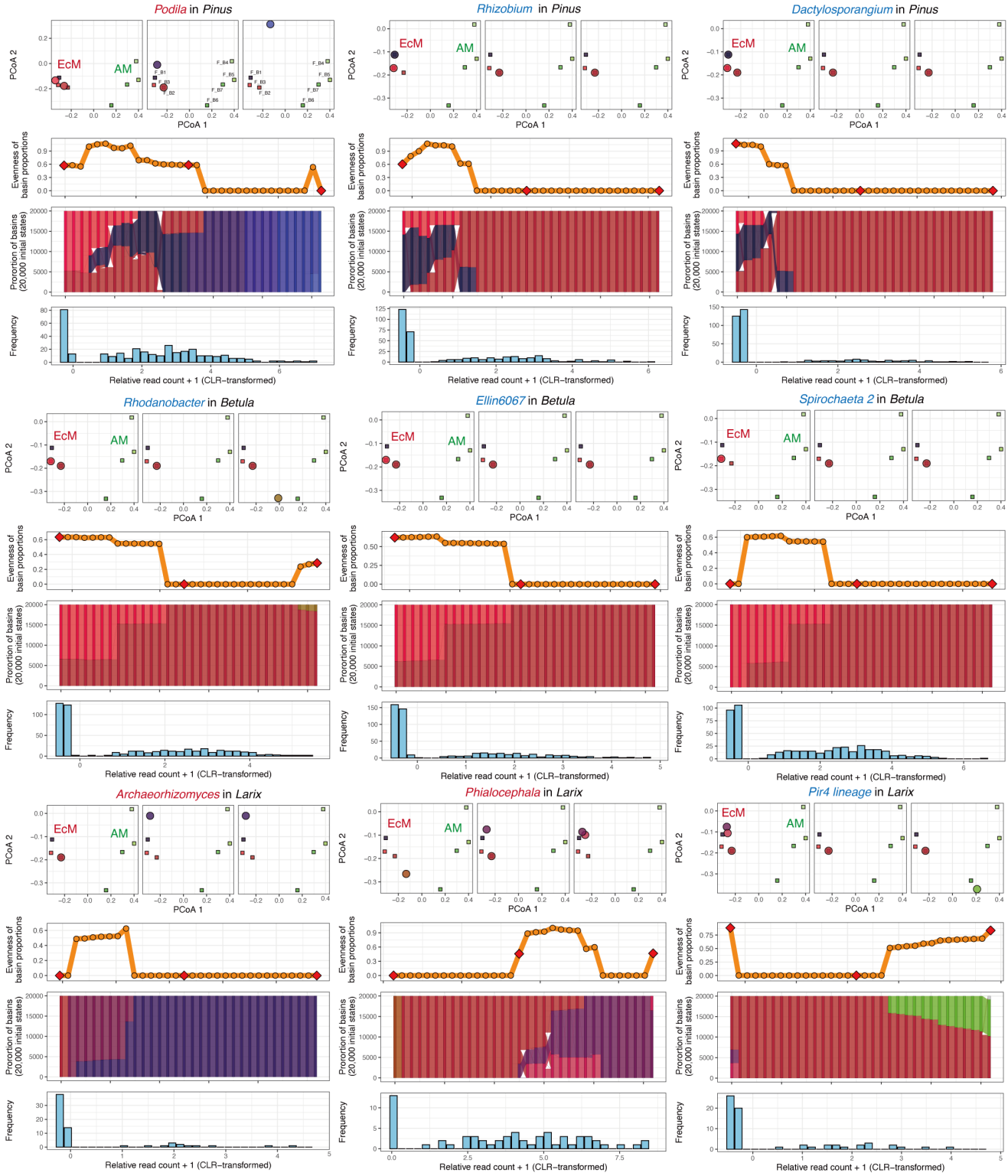

335

336 **Supplementary Fig. S22 | Fungal energy landscape reorganization in the ectomycorrhizal host-**
337 **plant backgrounds.** Along the abundance gradient of each microbial genus highlighted in figure 4b
338 (*Pinus*, *Betula* and *Larix*), changes in the frequency distribution of fungal energy landscape basins are
339 shown. Frequencies are evaluated through 20,000 simulations of community assemblies from
340 randomly generated initial states, under 32 abundance conditions ranging from absence to the
341 maximum observed abundance in the host. On the PCoA planes, the basin bottoms detected at three
342 representative abundance levels within 32 equally spaced relative abundance steps—absence (step 1),

intermediate abundance (step 16), and maximum abundance (step 32)—are shown as circles, together with the states detected in Figure 2c (see Supplementary Fig. S19a). The Shannon entropy of the basin frequencies is also shown along the abundance axis (CLR-transformed relative read counts of a focal genus). In addition, the destinations of the initial communities in each condition of the focal genus's abundance are indicated in the flow diagrams with the histograms of their relative abundances in the hosts. Each bar plot depicts the frequency of basin bottoms detected under the corresponding abundance condition. The bottoms which the same initial community state converged across adjacent abundance conditions (steps) are connected with bands. Colors represent community compositional similarity based on Jaccard distance, with more similar compositions rendered in more similar colors (see Fig. 2c; Supplementary Fig. S20).

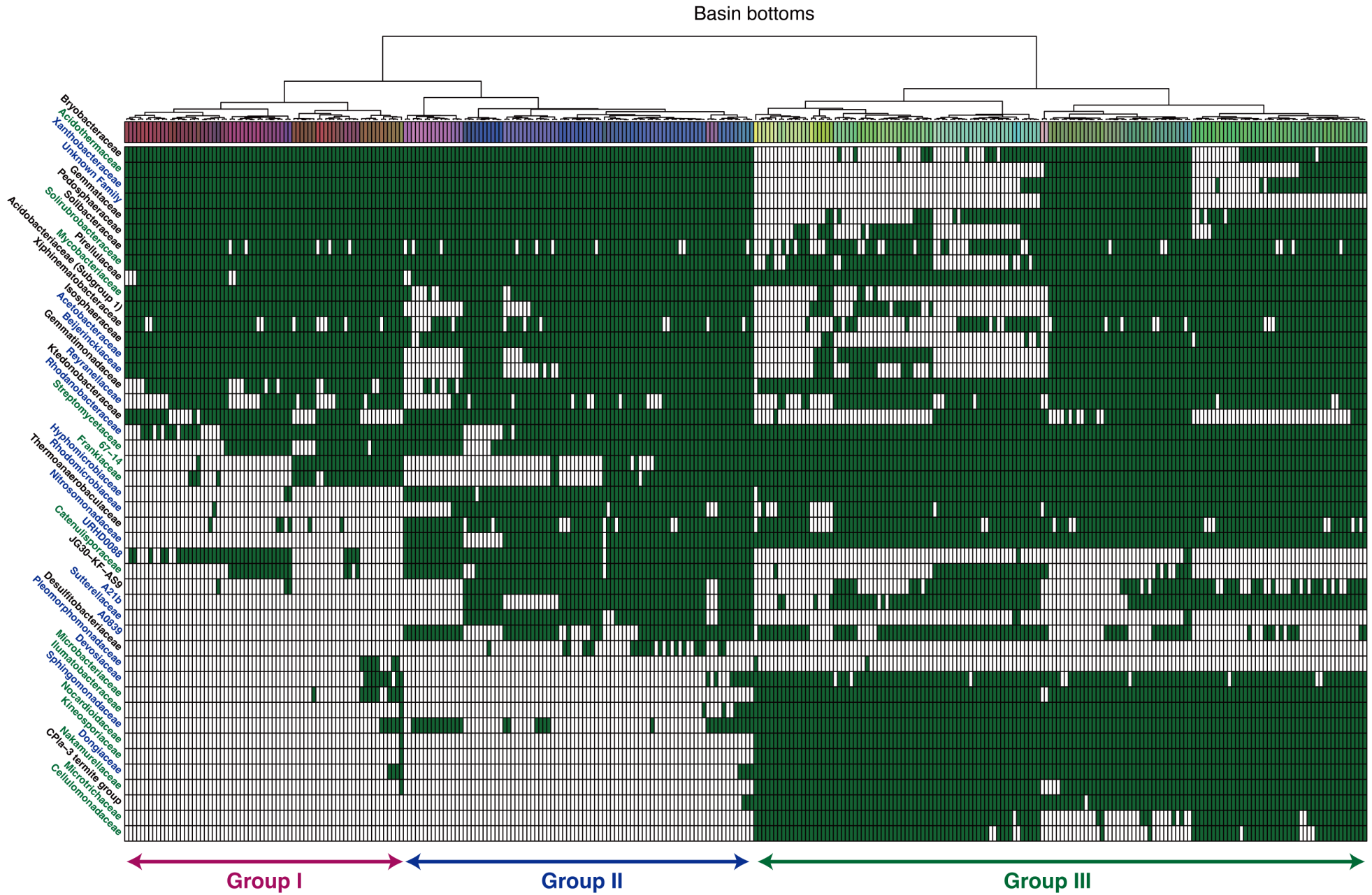
Basin bottoms
Bryobacteraceae
Acidothermaceae
Xanthobacteraceae
Unknown Family
Gemmataceae
Pedosphaeraceae
Solibacteraceae
Solirubrobacteraceae
Mycobacteriaceae
Pirellulaceae
Acidobacteriaceae (Subgroup 1)
Xiphinematobacteraceae
Isosphaeraceae
Acetobacteraceae
Beijerinckiaceae
Gemmatimonadaceae
Reyranellaceae
Ktedonobacteraceae
Rhodanobacteraceae
Streptomycetaceae
Frankiaceae
67-14
Hyphomicrobiaceae
Rhodomicrobiaceae
Thermoanaerobaculaceae
Nitrosomonadaceae
URHD0088
Catenulisporaceae
JG30-KF-AS9
Sutterellaceae
A21b
Desulfitobacteriaceae
A0839
Pleomorphomonadaceae
Devosiaceae
Microbacteriaceae
Ilumatobacteraceae
Sphingomonadaceae
Nocardioidaceae
Kineosporiaceae
Dongiaceae
Nakamurellaceae
CPla-3 termite group
Micrococcaceae
Cellulomonadaceae
Group I
Group II
Group III

Supplementary Fig. S23 | Community states at basin bottoms of prokaryotic energy landscapes. The basin bottoms inferred across the six host plant backgrounds in Figures 3c and 6, Supplementary Figures S24 and S25 are shown with a dendrogram representing taxonomic membership similarity. The color gradient of left-side panel represents the degree of similarity/dissimilarity among community states, corresponding to those illustrated in the flow diagrams (see Fig. 6 and Supplementary Figs. S24 and S25). The basins are tentatively classified into three categories: Group I, consisting primarily of commonly observed families; Group II, characterized by the presence of additional Pseudomonadota families; and Group III, characterized by the presence of additional Actinomycetota families. Prokaryotic families are colored according to their phylum-level taxonomy: blue, Pseudomonadota; green, Actinomycetota; black, other phyla.

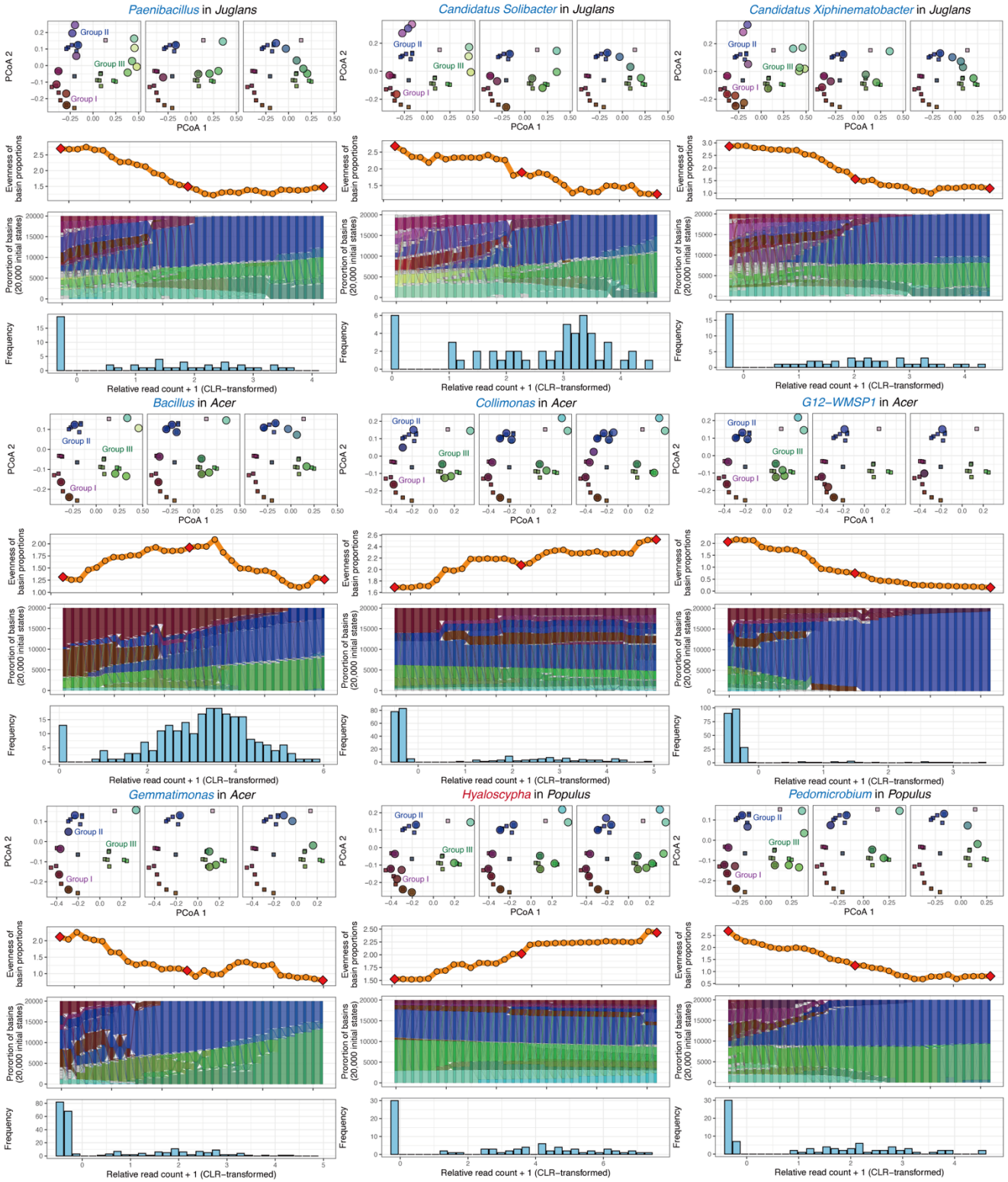

Supplementary Fig. S24 | Prokaryotic energy landscape reorganization in the dual mycorrhizal host-plant backgrounds. Along the abundance gradient of each microbial genus highlighted in Figure 4d (*Juglans*, *Acer* and *Populus*), changes in the frequency distribution of prokaryotic energy landscape basins are shown. Frequencies are evaluated through 20,000 simulations of community assemblies from randomly generated initial states, under 32 abundance conditions ranging from absence to the maximum observed abundance in the host. On the PCoA planes, the basin bottoms detected at three representative abundance levels within 32 equally spaced relative abundance steps—

absence (step 1), intermediate abundance (step 16), and maximum abundance (step 32)—are shown as circles, together with the states detected in Figure 3c (see Supplementary Fig. S19b). The Shannon entropy of the basin frequencies is also shown along the abundance axis (CLR-transformed relative read counts of a focal genus). In addition, the destinations of the initial communities in each condition of the focal genus's abundance are indicated in the flow diagrams with the histograms of their relative abundances in the hosts. Each bar plot depicts the frequency of basin bottoms detected under the corresponding abundance condition. The bottoms which the same initial community state converged across adjacent abundance conditions (steps) are connected with bands. Colors represent community compositional similarity based on Jaccard distance, with more similar compositions rendered in more similar colors (see Fig. 3c; Supplementary Fig. S23).

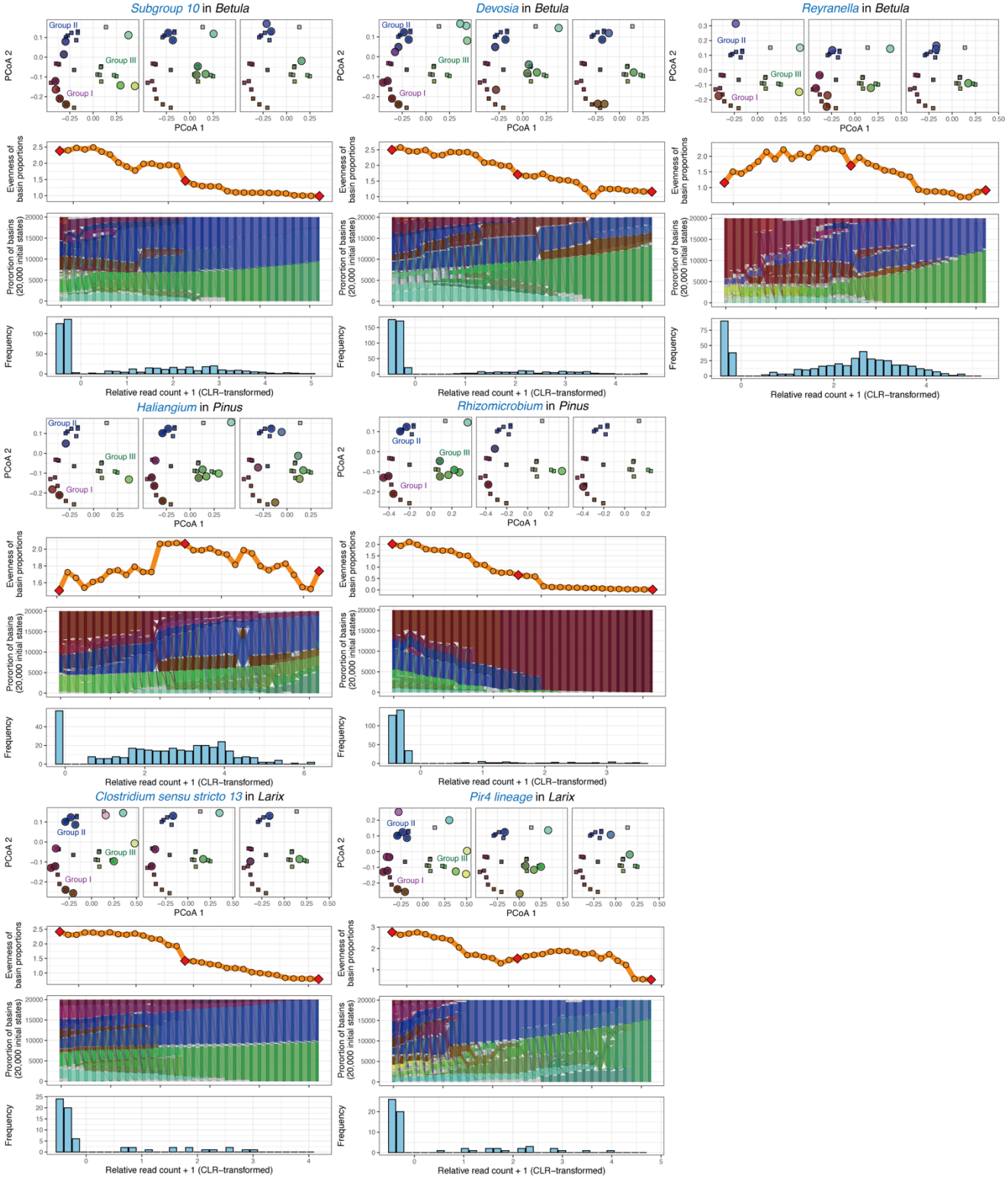

382

383 **Supplementary Fig. S25 | Prokaryotic energy landscape reorganization in the ectomycorrhizal**
384 **host-plant backgrounds.** Along the abundance gradient of each microbial genus highlighted in
385 Figure 4d (*Betula, Pinus*, and *Larix*), changes in the frequency distribution of prokaryotic energy
386 landscape basins are shown. Frequencies are evaluated through 20,000 simulations of community
387 assemblies from randomly generated initial states, under 32 abundance conditions ranging from
388 absence to the maximum observed abundance in the host. On the PCoA planes, the basin bottoms

detected at three representative abundance levels within 32 equally spaced relative abundance steps—absence (step 1), intermediate abundance (step 16), and maximum abundance (step 32)—are shown as circles, together with the states detected in Figure 3c (see Supplementary Fig. S19b). The Shannon entropy of the basin frequencies is also shown along the abundance axis (CLR-transformed relative read counts of a focal genus). In addition, the destinations of the initial communities in each condition of the focal genus's abundance are indicated in the flow diagrams with the histograms of their relative abundances in the hosts. Each bar plot depicts the frequency of basin bottoms detected under the corresponding abundance condition. The bottoms which the same initial community state converged across adjacent abundance conditions (steps) are connected with bands. Colors represent community compositional similarity based on Jaccard distance, with more similar compositions rendered in more similar colors (see Fig. 3c; Supplementary Fig. S23).

Supplementary Table S1 | Prioritization of fungal families based on their contributions to overall community structure. To select candidate family sets for subsequent analyses (see Supplementary Figs. S1 and S3), individual fungal families were prioritized according to their explanatory power for the abundance-based fungal community structure. Specifically, a PerMANOVA was performed on the relative abundance matrix of fungal data using the presence/absence of each family as an explanatory variable (10,000 iterations). In the PerMANOVA, Bray-Curtis distance was used to quantify community dissimilarity between root samples, and the host plant backgrounds and sampling points were included as additional explanatory variables (i.e., covariates).

Family	R^2	P (FDR)
Russulaceae	3.76×10^{-2}	< 0.001
Thelephoraceae	1.50×10^{-2}	< 0.001
Hydnaceae	1.30×10^{-2}	< 0.001
Tricholomataceae	1.26×10^{-2}	< 0.001
Hyaloscyphaceae	1.12×10^{-2}	< 0.001
Glomeraceae	1.11×10^{-2}	< 0.001
Mollisiaceae	1.08×10^{-2}	< 0.001
Mycenaceae	9.92×10^{-3}	< 0.001
Herpotrichiellaceae	8.50×10^{-3}	< 0.001
Clavariaceae	6.55×10^{-3}	< 0.001
Dermateaceae	5.53×10^{-3}	< 0.001
Cephalothecaceae	5.24×10^{-3}	< 0.001
Amanitaceae	4.74×10^{-3}	< 0.001
Helotiaceae	4.49×10^{-3}	< 0.001
Mortierellaceae	4.44×10^{-3}	< 0.001
Hymenogastraceae	4.32×10^{-3}	< 0.001
Helotiales_fam_Incertae_sedis	4.31×10^{-3}	< 0.001
Inocybaceae	3.84×10^{-3}	< 0.001
Tarzettaceae	3.47×10^{-3}	< 0.001
Leotiaceae	3.42×10^{-3}	< 0.001
Myxotrichaceae	3.42×10^{-3}	< 0.001
Ceratobasidiaceae	3.40×10^{-3}	< 0.001
Archaeorhizomycetaceae	2.76×10^{-3}	< 0.001
Cortinariaceae	2.71×10^{-3}	< 0.001
Rozellomycota_fam_Incertae_sedis	2.70×10^{-3}	< 0.001
Strophariaceae	2.64×10^{-3}	< 0.001
Sebacinaceae	2.61×10^{-3}	< 0.001
Aspergillaceae	2.27×10^{-3}	< 0.001
Hydnangiaceae	2.25×10^{-3}	0.001
Pyronemataceae	2.24×10^{-3}	< 0.001

Geoglossaceae	2.21×10^{-3}	< 0.001
Trimorphomycetaceae	2.20×10^{-3}	0.002
Tylosporaceae	2.20×10^{-3}	< 0.001
Tremellodendropsidales_fam_Incertae_sedis	2.12×10^{-3}	< 0.001
Ramicandelaberales_fam_Incertae_sedis	2.05×10^{-3}	0.002
Entolomataceae	1.92×10^{-3}	0.001
Leucosporidiales_fam_Incertae_sedis	1.91×10^{-3}	< 0.001
Pezizaceae	1.85×10^{-3}	0.003
Tuberaceae	1.83×10^{-3}	< 0.001
Venturiaceae	1.76×10^{-3}	0.007
Trichosporonaceae	1.72×10^{-3}	0.004
Leptodontidiaceae	1.69×10^{-3}	0.010
Melanommataceae	1.58×10^{-3}	0.008
Psathyrellaceae	1.57×10^{-3}	0.009
Endogonaceae	1.51×10^{-3}	0.006
Cladosporiaceae	1.46×10^{-3}	0.015
Clavicipitaceae	1.43×10^{-3}	0.005
Hypocreaceae	1.43×10^{-3}	0.016
Nectriaceae	1.39×10^{-3}	0.008
Umbelopsidaceae	1.38×10^{-3}	0.014
Microbotryales_fam_Incertae_sedis	1.27×10^{-3}	0.017
Cordycipitaceae	1.24×10^{-3}	0.017
Piskurozymaceae	1.23×10^{-3}	0.016
GS11_fam_Incertae_sedis	1.20×10^{-3}	0.013
Pleosporaceae	1.19×10^{-3}	0.042
Mytilinidiaceae	1.06×10^{-3}	0.048

408

Supplementary Table S2 | Prioritization of prokaryotic families based on their contributions to overall community structure. To select candidate family sets for subsequent analyses (see Supplementary Figs. S1 and S3), individual prokaryotic families were prioritized according to their explanatory power for the abundance-based prokaryotic community structure. Specifically, a PerMANOVA was performed on the relative abundance matrix of prokaryotic data, using the presence/absence of each family as an explanatory variable (10,000 iterations). In the PerMANOVA, Bray-Curtis distance was used to quantify community dissimilarity between root samples, and the host plant backgrounds and sampling points were included as additional explanatory variables (i.e., covariates).

Family	R^2	*P* (FDR)
Microbacteriaceae	2.10×10^{-2}	< 0.001
Kineosporiaceae	1.97×10^{-2}	< 0.001
Dongiaceae	1.97×10^{-2}	< 0.001
67-14	1.89×10^{-2}	< 0.001
Catenulisporaceae	1.79×10^{-2}	< 0.001
Ktedonobacteraceae	1.75×10^{-2}	< 0.001
Nocardioidaceae	1.70×10^{-2}	< 0.001
Xanthobacteraceae	1.56×10^{-2}	< 0.001
JG30-KF-AS9	1.48×10^{-2}	< 0.001
Hyphomicrobiaceae	1.42×10^{-2}	< 0.001
Sutterellaceae	1.39×10^{-2}	< 0.001
Frankiaceae	1.36×10^{-2}	< 0.001
Solibacteraceae	1.32×10^{-2}	< 0.001
Unknown Family	1.29×10^{-2}	< 0.001
Acetobacteraceae	1.27×10^{-2}	< 0.001
Nakamurellaceae	1.27×10^{-2}	< 0.001
Devosiaceae	1.23×10^{-2}	< 0.001
Thermoanaerobaculaceae	1.15×10^{-2}	< 0.001
URHD0088	1.13×10^{-2}	< 0.001
Beijerinckiaceae	1.12×10^{-2}	< 0.001
Microtrichaceae	1.12×10^{-2}	< 0.001
Solirubrobacteraceae	1.11×10^{-2}	< 0.001
Cellulomonadaceae	1.08×10^{-2}	< 0.001
Isosphaeraceae	1.05×10^{-2}	< 0.001
Pirellulaceae	1.05×10^{-2}	< 0.001
Xiphinematobacteraceae	1.03×10^{-2}	< 0.001
Acidothermaceae	1.03×10^{-2}	< 0.001
Nitrosomonadaceae	1.02×10^{-2}	< 0.001
Pedosphaeraceae	1.02×10^{-2}	< 0.001

Desulfitobacteriaceae	9.98×10^{-3}	< 0.001
A21b	9.65×10^{-3}	< 0.001
Bryobacteraceae	9.62×10^{-3}	< 0.001
Rhodomicrobiaceae	9.47×10^{-3}	< 0.001
Streptomycetaceae	9.37×10^{-3}	< 0.001
Acidobacteriaceae (Subgroup 1)	9.35×10^{-3}	< 0.001
Rhodanobacteraceae	9.28×10^{-3}	< 0.001
Sphingomonadaceae	9.24×10^{-3}	< 0.001
Pleomorphomonadaceae	9.22×10^{-3}	< 0.001
A0839	9.19×10^{-3}	< 0.001
CPla-3 termite group	9.13×10^{-3}	< 0.001
Ilumatobacteraceae	9.13×10^{-3}	< 0.001
Gemmatimonadaceae	9.07×10^{-3}	< 0.001
Reyranellaceae	8.88×10^{-3}	< 0.001
Gemmataceae	8.82×10^{-3}	< 0.001
Mycobacteriaceae	8.80×10^{-3}	< 0.001
Rhizobiaceae	8.32×10^{-3}	< 0.001
Micromonosporaceae	8.16×10^{-3}	< 0.001
Paenibacillaceae	8.03×10^{-3}	< 0.001
Burkholderiaceae	8.03×10^{-3}	< 0.001
Vermiphilaceae	7.94×10^{-3}	< 0.001
SC-I-84	7.90×10^{-3}	< 0.001
Legionellaceae	7.86×10^{-3}	< 0.001
Steroidobacteraceae	7.78×10^{-3}	< 0.001
WD2101 soil group	7.66×10^{-3}	< 0.001
Labraceae	7.65×10^{-3}	< 0.001
Microscillaceae	7.62×10^{-3}	< 0.001
Gimesiaceae	7.45×10^{-3}	< 0.001
Sphingobacteriaceae	7.42×10^{-3}	< 0.001
Myxococcaceae	7.42×10^{-3}	< 0.001
Pseudonocardiaceae	7.41×10^{-3}	< 0.001
Comamonadaceae	7.37×10^{-3}	< 0.001
LWQ8	7.32×10^{-3}	< 0.001
Rhizobiales Incertae Sedis	7.27×10^{-3}	< 0.001
Anaerolineaceae	7.03×10^{-3}	< 0.001
Polyangiaceae	7.02×10^{-3}	< 0.001
Oxalobacteraceae	6.71×10^{-3}	< 0.001
Magnetospirillaceae	6.71×10^{-3}	< 0.001
Spirochaetaceae	6.69×10^{-3}	< 0.001
Hyphomonadaceae	6.64×10^{-3}	< 0.001

Sporichthyaceae	6.40×10^{-3}	< 0.001
Blastocatellaceae	6.03×10^{-3}	< 0.001
Methylacidiphilaceae	6.02×10^{-3}	< 0.001
env.OPS 17	6.01×10^{-3}	< 0.001
WWH38	5.91×10^{-3}	< 0.001
Saccharimonadaceae	5.71×10^{-3}	< 0.001
Anaeromyxobacteraceae	5.55×10^{-3}	< 0.001
Chthoniobacteraceae	5.52×10^{-3}	< 0.001
Bacillaceae	5.42×10^{-3}	< 0.001
Lachnospiraceae	5.34×10^{-3}	< 0.001
Micropepsaceae	5.21×10^{-3}	< 0.001
Opitutaceae	5.08×10^{-3}	< 0.001
Clostridiaceae	5.07×10^{-3}	< 0.001
Actinospicaceae	5.07×10^{-3}	< 0.001
Caulobacteraceae	4.96×10^{-3}	< 0.001
KF-JG30-B3	4.81×10^{-3}	< 0.001
Phycisphaeraceae	4.79×10^{-3}	< 0.001
JG30-KF-CM45	4.78×10^{-3}	< 0.001
Chthonomonadaceae	4.76×10^{-3}	< 0.001
Koribacteraceae	4.70×10^{-3}	< 0.001
Haliangiaceae	4.54×10^{-3}	< 0.001
Sandaracinaceae	4.44×10^{-3}	< 0.001
Parvibaculaceae	4.35×10^{-3}	< 0.001
Pyrinomonadaceae	4.34×10^{-3}	< 0.001
Xanthomonadaceae	4.27×10^{-3}	< 0.001
Bdellovibrionaceae	4.22×10^{-3}	< 0.001
Simkaniaceae	4.15×10^{-3}	< 0.001
Parachlamydiaceae	4.13×10^{-3}	< 0.001
BIrii41	4.04×10^{-3}	< 0.001
A4b	3.99×10^{-3}	< 0.001
Pseudomonadaceae	3.76×10^{-3}	< 0.001
Phaselicystidaceae	3.74×10^{-3}	< 0.001
Chitinophagaceae	3.72×10^{-3}	< 0.001
SM2D12	3.67×10^{-3}	< 0.001
Thermomonosporaceae	3.65×10^{-3}	< 0.001
Rhodospirillaceae	3.63×10^{-3}	< 0.001
Amoebophilaceae	3.60×10^{-3}	< 0.001
CWT CU03-E12	3.60×10^{-3}	< 0.001
Nitrospiraceae	3.57×10^{-3}	< 0.001
Alicyclobacillaceae	3.54×10^{-3}	< 0.001

Inquilinaceae	3.53×10^{-3}	< 0.001
cvE6	3.53×10^{-3}	< 0.001
Coxiellaceae	3.50×10^{-3}	< 0.001
Verrucomicrobiaceae	3.45×10^{-3}	< 0.001
Elsteraceae	3.38×10^{-3}	< 0.001
UBA12409	3.37×10^{-3}	< 0.001
Chlamydiaceae	3.29×10^{-3}	< 0.001
Flavobacteriaceae	3.26×10^{-3}	< 0.001
Obscuribacteraceae	3.21×10^{-3}	< 0.001
Gaiellaceae	3.19×10^{-3}	< 0.001
Vicinamibacteraceae	3.10×10^{-3}	< 0.001
Propionibacteriaceae	3.03×10^{-3}	< 0.001
WX65	3.02×10^{-3}	< 0.001
Thermoactinomycetaceae	3.02×10^{-3}	< 0.001
Babeliaceae	2.99×10^{-3}	< 0.001
Fimbriimonadaceae	2.87×10^{-3}	< 0.001
Diplorickettsiaceae	2.82×10^{-3}	< 0.001
TRA3-20	2.75×10^{-3}	< 0.001
AKYH767	2.74×10^{-3}	< 0.001
Holosporaceae	2.71×10^{-3}	< 0.001
Schlesneriaceae	2.62×10^{-3}	< 0.001
37-13	2.59×10^{-3}	< 0.001
Methyloligellaceae	2.56×10^{-3}	< 0.001
Peptostreptococcaceae	2.49×10^{-3}	< 0.001
Moraxellaceae	2.42×10^{-3}	< 0.001
Terrimicrobiaceae	2.28×10^{-3}	< 0.001
Iamiaceae	2.27×10^{-3}	< 0.001
Leptospiraceae	2.27×10^{-3}	0.002
Azospirillaceae	2.24×10^{-3}	0.002
Paracaedibacteraceae	2.14×10^{-3}	< 0.001
Rickettsiaceae	2.12×10^{-3}	< 0.001
Planococcaceae	2.12×10^{-3}	0.001
Candidatus Jidaibacter	2.10×10^{-3}	0.001
Streptosporangiaceae	1.95×10^{-3}	0.002
Armatimonadaceae	1.91×10^{-3}	< 0.001
Rhodobacteraceae	1.88×10^{-3}	0.008
Yersiniaceae	1.87×10^{-3}	0.008
Erysipelotrichaceae	1.86×10^{-3}	0.001
KD3-93	1.81×10^{-3}	0.005
Acholeplasmataceae	1.68×10^{-3}	0.002

Rhodocyclaceae	1.66×10^{-3}	0.003
Oligoflexaceae	1.62×10^{-3}	0.002
YM_S32_TM7_50_20	1.60×10^{-3}	0.002
Cytophagaceae	1.60×10^{-3}	0.003
Vampirovibrionaceae	1.48×10^{-3}	0.006
Nocardiaceae	1.47×10^{-3}	0.011
Chitinimonadaceae	1.41×10^{-3}	0.011
type III	1.40×10^{-3}	0.006
Intrasporangiaceae	1.39×10^{-3}	0.029
NS11-12 marine group	1.30×10^{-3}	0.034
Ruminococcaceae	1.28×10^{-3}	0.007
Solimonadaceae	1.21×10^{-3}	0.016
Neisseriaceae	1.15×10^{-3}	0.021
Micavibrionaceae	1.06×10^{-3}	0.029
Puniceicoccaceae	1.02×10^{-3}	0.032

418

Supplementary Table S3 | Genera that exhibited the greatest potential impacts on the fungal assembly landscape along their abundance gradients. The *Δtopography* and *Δevenness* indices respectively represented changes in the overall topography and evenness of energy landscape architecture along the abundance gradients of a focal genus (from absence to their median abundance condition; Fig. 1d-g). The *z*-standardized metrics of *Δtopography* and *Δevenness* are obtained based on the randomization analysis in which the abundance of a focal genus was shuffled within the root samples of the same host plant (10,000 iterations). For each host plant background, the two fungal/prokaryotic genera with the highest and significant *Δtopography* are listed.

Genus	Host plant	z-standardized *Δtopography*	*P* (FDR) [*Δtopography*]	z-standardized *Δevenness*	*P* (FDR) [*Δevenness*]
Hyaloscypha	*Betula*	4.33	**< 0.001**	-1.63	0.170
Spirochaeta 2	*Betula*	3.47	**< 0.001**	0.05	0.517
Podila	*Pinus*	1.03 ×10	**< 0.001**	-0.19	0.482
Rhizobium	*Pinus*	6.57	**< 0.001**	-2.01	0.063
Oidiodendron	*Acer*	1.93 ×10	**< 0.001**	-4.84	0.030
Podila	*Acer*	9.42	**< 0.001**	1.13	0.252
Cladophialophora	*Populus*	2.50 ×10	**< 0.001**	8.63	**0.002**
Pezicula	*Populus*	1.36 ×10	**< 0.001**	2.56	0.129
Oidiodendron	*Larix*	1.18 ×10	**0.001**	2.38 ×10	**0.005**
Archaeorhizomyces	*Larix*	7.94	**< 0.001**	0.06	0.703
Hyaloscypha	*Juglans*	8.43	**< 0.001**	3.45	**0.002**
Meliniomyces	*Juglans*	8.16	**< 0.001**	0.97	0.290

Supplementary Table S4 | Ectomycorrhizal fungal genera for which significant impacts on the fungal assembly landscape were inferred. The *Δtopography* and *Δevenness* indices respectively represented changes in the overall topography and evenness of energy landscape architecture along the abundance gradients of a focal genus (from absence to their median abundance condition; Fig. 1d-g). The *z*-standardized metrics of *Δtopography* and *Δevenness* are obtained based on the randomization analysis in which the abundance of a focal genus was shuffled within the root samples of the same host plant (10,000 iterations). The ectomycorrhizal genera exhibited significant Δ*topography* are listed.

Genus	Host plant	z-standardized *Δtopography*	*P* (FDR) [*Δtopography*]	z-standardized *Δevenness*	*P* (FDR) [*Δevenness*]
Amanita	*Populus*	8.83	**< 0.001**	3.23	0.081
Russula	*Acer*	4.38	**< 0.001**	2.55	**0.020**
Russula	*Juglans*	4.10	**< 0.001**	-1.89	0.086
Tomentella	*Populus*	2.87	**< 0.001**	2.27	0.081
Russula	*Pinus*	4.24	**0.001**	1.21	0.155
Thelephora	*Populus*	6.73	**0.001**	1.47	0.192
Tomentella	*Juglans*	3.19	**0.001**	-1.72	0.123
Sebacina	*Acer*	3.64	**0.002**	0.99	0.311
Amanita	*Larix*	4.85	**0.006**	0.89	0.311
Amanita	*Acer*	2.85	**0.007**	-0.45	0.372
Amanita	*Pinus*	3.14	**0.009**	-2.43	0.098
Sebacina	*Larix*	2.84	**0.012**	2.79	**0.025**
Tricholoma	*Betula*	1.60	**0.027**	-1.49	0.365
Thelephora	*Larix*	4.17	**0.029**	-0.28	0.710
Lactarius	*Acer*	2.09	**0.030**	1.77	0.151
Sebacina	*Pinus*	2.39	**0.035**	-2.14	0.148
Thelephora	*Pinus*	2.19	**0.042**	-2.26	0.157
Lactarius	*Larix*	3.52	**0.048**	-0.59	0.687

Supplementary Table S5 | Genera that exhibited the greatest potential impacts on the prokaryotic assembly landscape along their abundance gradients. The *Δtopography* and *Δevenness* indices respectively represented changes in the overall topography and evenness of energy landscape architecture along the abundance gradients of a focal genus (from absence to their median abundance condition; Fig. 1d-g). The *z*-standardized metrics of *Δtopography* and *Δevenness* are obtained based on the randomization analysis in which the abundance of a focal genus was shuffled within the root samples of the same host plant (10,000 iterations). For each host plant background, the two fungal/prokaryotic genera with the highest and significant *Δtopography* are listed.

Genus	Host plant	z-standardized *Δtopography*	*P* (FDR) [*Δtopography*]	z-standardized *Δevenness*	*P* (FDR) [*Δevenness*]
Candidatus Udaeobacter	*Betula*	2.70×10	**< 0.001**	-2.76	**0.020**
Candidatus Solibacter	*Betula*	2.67×10	**< 0.001**	3.94	**0.005**
Candidatus Udaeobacter	*Pinus*	2.63×10	**< 0.001**	4.49×10^{-5}	0.532
Candidatus Solibacter	*Pinus*	2.17×10	**< 0.001**	1.77	0.124
Candidatus Solibacter	*Acer*	2.34×10	**< 0.001**	2.57	0.039
Candidatus Udaeobacter	*Acer*	2.31×10	**< 0.001**	-0.42	0.434
Candidatus Udaeobacter	*Populus*	3.02×10	**< 0.001**	-3.02	**0.012**
Candidatus Solibacter	*Populus*	2.75×10	**< 0.001**	-2.73	0.029
Candidatus Udaeobacter	*Larix*	2.64×10	**< 0.001**	-2.00	0.090
Candidatus Solibacter	*Larix*	2.26×10	**< 0.001**	-0.51	0.407
Candidatus Udaeobacter	*Juglans*	3.26×10	**< 0.001**	-8.18	**0.002**
Candidatus Solibacter	*Juglans*	2.93×10	**< 0.001**	-8.42	**0.002**

Supplementary Table S6 | Genera that exhibited the greatest potential impacts on the fungal assembly landscape at the 25% quantiles of their abundance. The z-standardized *Δtopography* and *Δevenness* indices respectively calculated along the abundance gradients of a focal genus (from absence to their 25% quantiles of their abundances within the detected samples; Fig. 1d-g). For each host plant background, the two fungal/prokaryotic genera with the highest and significant *Δtopography* are listed.

Genus	Host plant	z-standardized *Δtopography*	*P* (FDR) [*Δtopography*]	z-standardized *Δevenness*	*P* (FDR) [*Δevenness*]
Archaeorhizomyces	*Acer*	8.12	**< 0.001**	-1.44	0.091
Haliangium	*Acer*	7.16	**< 0.001**	-3.35	0.026
Hyaloscypha	*Betula*	4.30	**< 0.001**	-2.09	0.107
Podila	*Betula*	3.10	**< 0.001**	-0.74	0.287
Hyaloscypha	*Juglans*	9.58	**< 0.001**	3.86	**0.002**
Haliangium	*Juglans*	6.85	**< 0.001**	-2.48	0.035
Oidiodendron	*Larix*	6.20	**< 0.001**	6.11×10	**0.002**
Podila	*Larix*	1.08	**0.001**	6.58	**0.002**
Podila	*Pinus*	1.05	**< 0.001**	0.48	0.301
Cladophialophora	*Pinus*	8.92	**< 0.001**	0.27	0.112
Cladophialophora	*Populus*	1.95×10	**< 0.001**	2.34	0.105
Pezicula	*Populus*	1.46	**< 0.001**	2.82	0.112

Supplementary Table S7 | Genera that exhibited the greatest potential impacts on the prokaryotic assembly landscape at the 25% quantiles of their abundance. The z-standardized *Δtopography* and *Δevenness* indices respectively calculated along the abundance gradients of a focal genus (from absence to their 25% quantiles of their abundances within the detected samples; Fig. 1d-g). For each host plant background, the two fungal/prokaryotic genera with the highest and significant *Δtopography* are listed.

Genus	Host plant	z-standardized *Δtopography*	*P* (FDR) [*Δtopography*]	z-standardized *Δevenness*	*P* (FDR) [*Δevenness*]
Candidatus Solibacter	*Acer*	2.31×10	**< 0.001**	1.88	0.120
Mycobacterium	*Acer*	2.22×10	**< 0.001**	-1.24	0.225
Pir4 lineage	*Betula*	2.56×10	**< 0.001**	-2.93	0.034
Candidatus Solibacter	*Betula*	2.53×10	**< 0.001**	8.14	**0.002**
Candidatus Udaeobacter	*Juglans*	3.27×10	**< 0.001**	-5.50	**0.002**
Candidatus Solibacter	*Juglans*	2.82×10	**< 0.001**	-5.24	**0.002**
Candidatus Udaeobacter	*Larix*	2.35×10	**< 0.001**	-1.90	0.106
Labrys	*Larix*	2.29×10	**< 0.001**	-0.36	0.447
Pir4 lineage	*Pinus*	2.18×10	**< 0.001**	-3.59	**0.007**
Candidatus Udaeobacter	*Pinus*	2.15×10	**< 0.001**	2.58	0.043
Candidatus Udaeobacter	*Populus*	2.96×10	**< 0.001**	-0.97	0.285
Candidatus Solibacter	*Populus*	2.80×10	**< 0.001**	-2.01	0.092

Supplementary Table S8 | Genera that exhibited the greatest potential impacts on the fungal assembly landscape at the 75% quantiles of their abundance. The z-standardized *Δtopography* and *Δevenness* indices respectively calculated along the abundance gradients of a focal genus (from absence to their 75% quantiles of their abundances within the detected samples; Fig. 1d-g). For each host plant background, the two fungal/prokaryotic genera with the highest and significant *Δtopography* are listed.

Genus	Host plant	z-standardized *Δtopography*	*P* (FDR) [*Δtopography*]	z-standardized *Δevenness*	*P* (FDR) [*Δevenness*]
Hyaloscypha	*Betula*	4.75	**< 0.001**	-1.19	0.387
Actinospica	*Betula*	3.55	**< 0.001**	0.19	0.419
Podila	*Pinus*	1.05×10	**< 0.001**	-2.04	0.045
Phialocephala	*Pinus*	7.32	**< 0.001**	-3.69	0.039
Oidiodendron	*Acer*	1.23×10	**< 0.001**	3.80	**0.016**
Podila	*Acer*	9.28	**< 0.001**	-0.94	0.246
Cladophialophora	*Populus*	2.48×10	**< 0.001**	9.56	**0.002**
Oidiodendron	*Populus*	1.65×10	**< 0.001**	-4.03	**0.020**
Cladophialophora	*Larix*	5.30×10	**< 0.001**	0.10	0.944
Phialocephala	*Larix*	1.52×10	**< 0.001**	3.30	0.049
Hyaloscypha	*Juglans*	1.02×10	**< 0.001**	5.25	**0.002**
Meliniomyces	*Juglans*	9.31	**< 0.001**	0.20	0.487

Supplementary Table S9 | Genera that exhibited the greatest potential impacts on the prokaryotic assembly landscape at the 75% quantiles of their abundance. The z-standardized *Δtopography* and *Δevenness* indices respectively calculated along the abundance gradients of a focal genus (from absence to their 75% quantiles of their abundances within the detected samples; Fig. 1d-g). For each host plant background, the two fungal/prokaryotic genera with the highest and significant *Δtopography* are listed.

Genus	Host plant	z-standardized *Δtopography*	P (FDR) [*Δtopography*]	z-standardized *Δevenness*	P (FDR) [*Δevenness*]
Candidatus Solibacter	*Betula*	2.66×10	**< 0.001**	1.97	0.115
Candidatus Udaeobacter	*Betula*	2.48×10	**< 0.001**	-3.66	**0.004**
Candidatus Udaeobacter	*Pinus*	2.57×10	**< 0.001**	-0.62	0.375
Candidatus Solibacter	*Pinus*	2.31×10	**< 0.001**	1.39	0.196
Candidatus Solibacter	*Acer*	2.50×10	**< 0.001**	1.02	0.285
Candidatus Udaeobacter	*Acer*	2.38×10	**< 0.001**	-1.63	0.151
Candidatus Solibacter	*Populus*	2.82×10	**< 0.001**	-4.23	**0.002**
Candidatus Udaeobacter	*Populus*	2.73×10	**< 0.001**	-4.90	**0.002**
Candidatus Udaeobacter	*Larix*	2.61×10	**< 0.001**	-4.86	**0.002**
Candidatus Solibacter	*Larix*	2.35×10	**< 0.001**	-3.93	**0.002**
Candidatus Udaeobacter	*Juglans*	3.07×10	**< 0.001**	-7.48	**0.002**
Candidatus Solibacter	*Juglans*	2.85×10	**< 0.001**	-7.74	**0.002**